# Direct repression of *Nanog* and *Oct4* by OTX2 modulates contribution of epiblast-derived cells to germline and somatic lineage

Luca Giovanni Di Giovannantonio[1†], Dario Acampora[1,†], Daniela Omodei[1,2], Vincenzo Nigro[3,4], Pasquale Barba[1], Elisa Barbieri[5, 6], Ian Chambers[5, 6] and Antonio Simeone[1,*]

[1]Institute of Genetics and Biophysics "Adriano Buzzati-Traverso", CNR, Via P. Castellino, 111, 80131 Naples, Italy; [2]Institute of Biostructures and Bioimaging, CNR, Via Tommaso De Amicis, 95, 80145 Naples, Italy; [3]Dipartimento di Medicina di Precisione, Università degli Studi della Campania "Luigi Vanvitelli", Via L. De Crecchio, 7, 80138 Naples, Italy; [4]Telethon Institute of Genetics and Medicine (TIGEM), Via Campi Flegrei, 34, 80087 Pozzuoli (NA), Italy; [5]Centre for Regenerative Medicine, Institute for Regeneration and Repair, University of Edinburgh, 5 Little France Drive, Edinburgh, EH16 4UU, Scotland; [6]Institute for Stem Cell Research, School of Biological Sciences, University of Edinburgh, Scotland.

† These authors equally contributed to the work

***Corresponding author:** antonio.simeone@igb.cnr.it; Tel. +39 081 6132401

**Key words:** Primordial Germ cells, *Otx2*, pluripotency Gene Regulatory Network

**ABSTRACT**

In mammals the pre-gastrula proximal epiblast gives rise to Primordial Germ Cells (PGCs) or somatic precursors in response to BMP4 and WNT signaling. Entry into the germline requires activation of a naïve-like pluripotency gene regulatory network (GRN). Recent work showed that suppression of OTX2 expression in the epiblast by BMP4 allows cells to develop a PGC fate in a precise temporal window. However, the mechanisms by which OTX2 suppresses PGC fate are unknown. Here we show that OTX2 prevents epiblast cells from activating the pluripotency GRN by direct repression of *Oct4* and *Nanog*. Loss of this control during PGC differentiation *in vitro* causes widespread activation of the pluripotency GRN and deregulated response to LIF, BMP4 and WNT signaling. These abnormalities, in specific cell culture conditions, result in massive germline entry at the expense of somatic mesoderm differentiation. Increased generation of PGCs occurs also in mutant embryos. We propose that the OTX2 repressive control of *Oct4* and *Nanog* is at the basis of the mechanism determining epiblast contribution to germline and somatic lineage.

## INTRODUCTION

Primordial Germ Cells (PGCs) represent the founder cells of the germ cell lineage which ensures the transmission of genetic and epigenetic information across the generations (Wylie, 1999; Surani, 2001; Saitou and Yamaji, 2012; Johnson et al., 2003; Johnson and Alberio, 2015). In mice, both the germline and the somatic lineage, the latter referring to embryonic and extraembryonic mesoderm (Saitou et al. 2005), originate from the proximal-posterior epiblast of pre-gastrula embryos (Lawson et al., 1999; Saitou, 2009). The generation of PGCs is controlled by a precise mechanism determining the segregation of the germline from the somatic lineage (Ohinata et al., 2009; Surani et al., 2007; Hayashi et al., 2007). The acquisition of PGC identity is associated with loss of somatic mesoderm fate (Günesdogan and Surani, 2016; Saitou et al., 2002). In mouse, germline and somatic lineage originate in response to BMP and WNT signaling (Lawson et al., 1999; Ohinata et al., 2009; Senft et al., 2019). BMP4-mediated activation of the Transcription Factors (TFs) *Blimp1* (also known as *Prdm1*), *Ap2γ* (also known as *Tfap2c*) and *Prdm14* is required for germline entry and suppression of somatic mesoderm identity, which is defined by the expression of *T* (also known as *Brachyury*) and *Hoxb1* (Magnúsdóttir et al., 2013; Ohinata et al., 2005; Kurimoto et al., 2008; Ancelin et al., 2006; Vincent et al., 2005; Weber et al., 2010; Yamaji et al., 2008; Nakaki et al., 2013). Co-expression of *Blimp1*, *Ap2γ*, and *Prdm14* defines the identity of germ cells *in vivo* and *in vitro*. Further work indicated that WNT3 is also required for PGC fate (Aramaki et al., 2013). Germline entry and development of PGCs also requires the activation of a naïve-like pluripotency gene regulatory network (GRN) defined by the TFs *Oct4* (also known as *Pou5f1*), *Sox2* and *Nanog* and representing a unique feature of the PGC unipotent state (Saitou and Yamaji, 2012; Hayashi et al., 2007; Hackett and Surani, 2014; Leitch et al., 2013; Smith, 2017; Okamura et al., 2008; Yamaguchi et al., 2009; Chambers et al., 2007; Zhang and Chambers, 2019; Campolo et al., 2013; Kehler et al., 2004; Yeom et al., 1996). Importantly, *Nanog* activation in epiblast-like cells (EpiLCs), a cellular state very similar to pre-gastrulation epiblast (Hayashi et al., 2011; Smith, 2017), is sufficient for germ cell induction (Murakami et al., 2016) and *Oct4* expression in PGCs requires a transcriptional regulatory switch from the proximal enhancer (PE) to the distal enhancer (DE) (Choi et al., 2016; Wu and Schöler, 2014). The study of germline development has been fueled by the realization of a stepwise *in vitro* culture system generating PGC-like cells (PGCLCs) from germline competent EpiLCs induced, in turn, from naïve embryonic stem cells (ESC) (Hayashi et al., 2011). PGCLCs and PGCs share molecular identity, epigenetic reprogramming and spermatogenic capacity (Hayashi et al., 2011, 2012, 2017). The TF OTX2, a key determinant of brain development (Acampora et al., 1995), is also expressed in pluripotent cells *in vivo* and *in vitro* (Acampora et al., 2013). OTX2 is required to: antagonize naïve pluripotency; promote transition of

ESCs from naïve to formative pluripotency; specify the heterogeneous identity of ESCs through reciprocal antagonism with NANOG; and define *in vitro* and *in vivo* naïve-primed intermediate states of pluripotency (Acampora et al., 2013, 2016, 2017 Buecker et al., 2014; Yang et al., 2014; Neagu et al., 2020). Moreover, in pluripotent cells OTX2 may also bind to the enhancer region of *Oct4*, *Nanog* and *Sox2* (Acampora et al., 2016). Recent work has revealed that OTX2 is a novel crucial determinant controlling germline entry of formative epiblast cells in mouse (Zhang et al., 2018; Zhang and Chambers, 2019; Laird, 2018). Indeed, by restricting germline entry to a limited number of epiblast-derived cells, OTX2 controls segregation of germ cells from somatic precursors. Here, we hypothesized that mechanistically, entry into germline requires the release by OTX2 of a repressive state preventing activation of the pluripotency GRN in epiblast-derived cells. Our data indicate that loss of OTX2 binding to *Oct4* or *Nanog* enhancer region causes in EpiLC-derived cells widespread activation of the pluripotency GRN, increased germline entry and suppression of somatic fate. Generation of PGCs is increased also in mutant embryos. This study uncovers a novel mechanism by which OTX2 regulates epiblast contribution to germline and somatic mesoderm.

## RESULTS

### OTX2, OCT4 and NANOG expression during PGC development and PGCLC differentiation

To obtain a detailed view of the temporal appearance of OTX2, OCT4 and NANOG relative to germline and somatic differentiation determinants, embryos were analysed by immunofluorescence (Fig.1A). At embryonic day (E) 6.5, AP2γ and BLIMP1 were co-expressed in a subset of FRAGILIS$^{+}$ (also known as *Ifitm3*) cells, which included incipient PGCs (Zhang et al., 2018). From E7 to E7.5 these three markers gradually became co-localized in PGCs (yellow arrows in Fig. 1A). At E6.5 and E7, OTX2 was expressed in some FRAGILIS$^{+}$-AP2γ$^{-}$ cells (white arrow in Fig. 1A), but became undetectable at E7.5 in FRAGILIS$^{+}$ cells. During this time window, OCT4 and NANOG were co-expressed in FRAGILIS$^{+}$ cells, though at E6.5 NANOG was detected at variable levels (Fig. 1A). T was initially expressed throughout the FRAGILIS$^{+}$ field but by E7.5 disappeared from some FRAGILIS$^{+}$ cells (Fig. 1A). These data show that AP2γ and BLIMP1 become expressed within FRAGILIS$^{+}$ cells only when OTX2 has been turned off suggesting that expression of OTX2 in FRAGILIS$^{+}$ cells may prevent precocious activation of AP2γ and BLIMP1.

To determine whether these temporal changes in expression were mirrored *in vitro*, we analysed EpiLC-derived cell aggregates during PGCLC differentiation by using a modification of the established procedure (Hayashi et al., 2011) in which the concentrations of BMP4, BMP8a, SCF and EGF were reduced ten-fold (protocol 1) as used previously (Zhang et al., 2018) (Fig. 1B).

AP2γ$^+$ cells were first detected at day (d) 0.5; at d1 some AP2γ$^+$ cells co-expressed BLIMP1 and these increased in number up to d2; OCT4 was expressed in all cells up to d1 with expression remaining high in AP2γ$^+$ cells at d2; NANOG was activated at high levels predominantly in AP2γ$^+$-T$^-$ cells; and T showed widespread activation beginning at d1 prevalently in AP2γ$^-$ cells expressing low level of NANOG (Fig. 1C). A comparison of OTX2 expression with that of OCT4, NANOG, AP2γ and T showed that, although markedly down-regulated between d0 and d1 (Zhang et al., 2018) and virtually undetectable at d2 (Fig. 1C), OTX2 remained detectable at d0.5 and d1 in numerous cells co-expressing OCT4 and low levels of NANOG and from d1 also T (Fig. 1C). Notably, at d0.5 OTX2 was absent from AP2γ$^+$ cells. This analysis confirms and extends previous finding (Zhang et al., 2018) indicating that during the germline and somatic differentiation time window, OTX2 is efficiently repressed in epiblast-derived or EpiLC-derived cells as they begin to differentiate towards PGCs or PGCLCs, while it is maintained for longer in somatic precursors. This suggests that differential OTX2 repression may prevent excessive germline differentiation.

**OTX2 binding to *Nanog* or *Oct4* enhancer region regulates the generation of PGCLCs and somatic cells**

To assess the hypothesis that differential OTX2 repression governs the extent of germline entry, we analysed ESCs in which specific OTX2 binding site(s) (Obs) were mutagenized. *Nanog*Δ*Obs3* ESCs have lost the strongest Obs (Obs3) in the *Nanog* enhancer (Acampora et al., 2016). In addition, we derived *Oct4*Δ*Obs* ESC lines mutagenized in the three Obs located in the enhancer region of *Oct4* (Fig. S1A-D): Obs1 within the PE, Obs2 at the 5' of the PE, and Obs3 at the 3' of the DE (Fig. S2A). Compared to wild type (wt), the OTX2 binding activity in *Oct4*Δ*Obs* ESCs and d2 EpiLCs was virtually abrogated (Fig. S2B). However, wt and *Oct4*Δ*Obs* ESCs showed no differences in self-renewal at clonal density (Fig. S2C; Table S1), expression of OCT4, NANOG, OTX2 and OCT6 (also known as *Pou3f1*) (Fig. S2D), ability to convert into the naïve state (Fig. S2E), steady state of LIF, FGF, WNT and BMP signaling (Fig. S2F), acute responsiveness to LIF (Fig. S2G) and FGF2 (Fig. S2H) and chimaera-forming capacity (Fig. S2I). Furthermore, analysis of *Oct4*Δ*Obs* and *Nanog*Δ*Obs3* EpiLCs at d2 showed uniform high level of OCT4, OTX2 and OCT6, absence of NANOG and T (Fig. S2J) and similar steady state levels of phospho (p)-ERK1,2, p-SMAD1,5,8, p-ßCATENIN, active ß-CATENIN and p-SMAD2 (Fig. S2K). Together these results indicate that *Oct4*Δ*Obs* ESCs and both *Oct4*Δ*Obs* and *Nanog*Δ*Obs3* EpiLCs are indistinguishable from wt cells.

To investigate whether *Oct4*Δ*Obs* and *Nanog*Δ*Obs3* (subsequently referred to as Δ*Obs*) ESCs are affected in their propensity to differentiate into germline cells, we employed the above mentioned protocol 1 as PGCLC differentiation method (Fig. 2A). FACS analysis (Fig. S3A-C) for SSEA1 (also known as *Fut4*) and CD61 (also known as *Itgb3*), which are co-expressed in PGCLCs, indicated that compared to wt, Δ*Obs* mutants generated at d6 a higher percentage of SSEA1$^{+}$-CD61$^{+}$ cells, approaching that of *Otx2* null (*Otx2KO*) cells (Zhang et al., 2018) (Fig. 2B). This finding was confirmed with independently generated Δ*Obs* cell lines (Fig. 2C). To determine whether increased generation of PGCLCs was presaged by altered expression of TFs, cytospin preparations of d2 cell aggregates were analyzed. Relative to wt, Δ*Obs* mutants showed an increased proportion of cells expressing high levels of OCT4, NANOG and BLIMP1 and a decreased proportion of T$^{+}$ cells (Fig. 2D; Fig. S3D,E; Table S2). Immunohistochemistry analysis of d2 cell aggregates supported cytospin data (Fig. 2E). Real-time quantitative PCR (RT-qPCR) analysis indicated that also the expression levels of *Oct4*, *Nanog*, *Ap2γ* and *Blimp1* were increased at d2 in mutants (Fig. 2F). For *Nanog* and *Blimp1* this was apparent at d0,5, for *Ap2γ* it was evident at d0.25 (Fig. 2F). No difference in *Otx2* expression was detected between wt and Δ*Obs* mutants, while the expression levels of *T* and *Hoxb1* were substantially diminished in Δ*Obs* mutants and virtually extinguished in *Otx2KO* cells (Fig. 2F,G). Previous studies reported that histone H3 tri-methyl lysine 9 (H3K9me3) is enriched at poised enhancers and may distinguish poised and active states for the DE and PE of *Oct4* (Wu and Schöler, 2014). Compared to wt, in *Oct4*Δ*Obs* d2 cell aggregates, the H3K9me3 level was reduced on the DE (Fig. 2H) suggesting a repressive role for OTX2 on DE activity. Increased generation of SSEA1$^{+}$-CD61$^{+}$ cells was observed in mutants also when PGCLC differentiation was initiated from ESCs maintained in serum plus LIF (protocol 2) (Fig. 2I,J; Fig. S4A). Therefore, in contrast to wt and similar to *Otx2KO* cells, germline differentiation of Δ*Obs* mutants is increased at the expense of somatic fate.

**Cytokine requirements for germline and somatic differentiation of Δ*Obs* mutants**

*Otx2KO* EpiLCs can undergo germline entry in the absence of cytokines (Zhang et al., 2018). To determine whether Δ*Obs* EpiLCs possessed the same capacity, we employed a cytokine-free differentiation protocol (protocol 3) (Fig. 3A). FACS analysis at d6 revealed moderate generation of PGCLCs only in *Otx2KO* cells (Fig. 3B). Cell counting and immunohistochemistry experiments showed that at d2 Δ*Obs* mutants significantly increased the percentage of total cells expressing high OCT4 and high NANOG and decreased the proportion of T$^{+}$ cells (Fig. 3C; Figs. S3D,E and S4B; Table S2). The BLIMP1$^{+}$ cell fraction was expanded only in *Otx2KO* cells. RT-qPCR analysis

showed that repression of *Otx2* was equally delayed in all genotypes and that expression of *Nanog*, *Oct4*, *Ap2γ*, *Blimp1*, and *T* at d2 was coherent with cell counting data (Fig. 3D). At earlier time points, the expression of these factors was similar in all genotypes except for *Blimp1* and *Ap2γ,* which were increased and precocious in *Otx2KO* cells (Zhang et al., 2018) (Fig. 3D). *Hoxb1* was inefficiently up-regulated in mutants (Fig. 3E). Therefore, in the absence of cytokines, Δ*Obs* mutants, in contrast to *Otx2KO* cells, are unable to promote germline differentiation. This suggests that cytokine-independent germline differentiation of Δ*Obs* mutants may require OTX2 functions in addition to those depending on OTX2 binding to *Oct4* or *Nanog* enhancer region. LIF is required for proliferation and survival of germ cells (Hayashi et al., 2011; Farini et al., 2005; Koshimizu et al., 1996; Cheng et al., 1994) and to maintain pluripotency and promote self-renewal of ESCs (Matsuda et al., 1999; Niwa et al., 2009). Since these functional properties may have an impact on germline differentiation of Δ*Obs* and *Otx2KO* mutants, we analyzed cell aggregates cultured with LIF only (protocol 4) (Fig. 4A). Compared to wt, Δ*Obs* and *Otx2KO* mutants generated more PGCLCs at d6 (Fig. 4B), and at d2 showed increased percentage of total cells expressing high OCT4, high NANOG and BLIMP1 and a virtual absence of $T^+$ cells (Fig. 4C; Figs. S3D,E and S4C; Table S2). RT-qPCR analysis showed that *Otx2* was efficiently repressed in all genotypes (Fig. 4D), while, compared to wt, in mutant cell aggregates *Oct4* expression was maintained high, *Blimp1*, *Ap2γ*, and *Nanog* were activated earlier, *T* and *Hoxb1* severely decreased (Fig. 4D,E). Therefore, LIF is sufficient to promote significant germline differentiation in Δ*Obs* mutants and, with a substantially higher efficiency, in *Otx2KO* cells.

To further investigate the contribution of LIF to PGCLC differentiation, we used a protocol in which LIF was the only component omitted from the cytokine cocktail (protocol 5) (Fig. 4F). Compared to wt, the number of PGCLCs at d6 was increased in Δ*Obs* and *Otx2KO* mutants (Fig. 4G). At d2 the percentage of total cells expressing high OCT4, high NANOG and BLIMP1 was significantly increased in all mutants, while the number of $T^+$ cells was strongly affected only in *Otx2KO* cells (Fig. 4H; Figs. S3D,E and S4D; Table S2). RT-qPCR analysis showed that repression of *Otx2* and activation of *Nanog*, *Blimp1* and *Ap2γ* were both less efficient than in protocols 1 and 4 (Fig. 4I). Compared to wt, *T* and *Hoxb1* activation was weakened in mutants (Fig. 4I,J). Taken together, findings from protocols 4 and 5 indicate that LIF alone provides a more effective stimulation of PGCLC differentiation than the remaining cytokines, and is particularly effective in suppressing somatic fate.

Previous work showed that endogenous WNT activity contributes to *Otx2* repression in different contexts and can be mimicked by the Glycogen synthase kinase 3 inhibitor (GSK3) CHIR99021 (CHIR) (Acampora et al., 2016; Neagu et al., 2020; Zhang et al., 2018). We therefore assessed

whether CHIR alone may stimulate the generation of PGCLCs and somatic mesoderm (protocol 6) (Fig. 5A). Only *Otx2KO* cells produced a substantial proportion of SSEA1$^{+}$-CD61$^{+}$ cells at d6 (Fig. 5B). Compared to wt and *Otx2KO* mutants, in Δ*Obs* mutants CHIR treatment generated intermediate percentages of cells expressing high OCT4, high NANOG and T (Fig. 5C; Figs. S3D,E and 5A; Table S3) and intermediate expression levels of *Oct4*, *Nanog*, *T* and *Hoxb1* (Fig. 5D,E). However in wt and Δ*Obs* mutants the percentage of BLIMP1$^{+}$ cells and the expression levels of *Blimp1* and *Ap2γ* were both similar to those described in cytokine-free culture conditions (Fig. 5C,D). RT-qPCR analysis showed that *Otx2* repression was comparable to that observed in protocol 5 (Fig. 5D). These results reveal that stimulation of the WNT pathway induces robust PGCLC differentiation only in *Otx2KO* cells, while in Δ*Obs* and *Otx2KO* mutants it efficiently suppresses somatic differentiation.

**LIF, WNT and BMP4 synergism promotes germline entry in Δ*Obs* mutants**

To determine whether WNT stimulation may synergize with LIF signaling during PGCLC differentiation, as reported for ESCs (ten Berge et al., 2011; Karwacki-Neisius et al., 2013; Ogawa et al., 2006), we assessed the effects of simultaneous addition of LIF and CHIR (protocol 7) (Fig. 5F). Compared to wt, the generation of PGCLCs at d6 was substantially higher in Δ*Obs* and *Otx2KO* mutants (Fig. 5G). This correlated with increased percentage of total cells expressing high OCT4, high NANOG and BLIMP1, severe decrease of T$^{+}$ cells (Fig. 5H; Figs. S3D,E and S5B; Table S3) and precocious and robust expression of *Nanog*, *Blimp1* and *Ap2γ* (Fig. 5I). In addition *T* and *Hoxb1* were not activated and *Otx2* was efficiently repressed (Fig. 5I,J). To explore whether low levels of stimulation of other pathways could likewise potentiate the effects of LIF, we assessed differentiation in the presence of LIF and a low dosage of BMP4, BMP8a, SCF and EGF (protocol 8) (Fig. 6A), whose concentrations were ten times lower than those used in protocols 1 and 5. Compared to wt, Δ*Obs* and *Otx2KO* mutants showed that PGCLC generation at d6 (Fig. 6B) and number of cells expressing at d2 high OCT4, high NANOG and BLIMP1 were both markedly increased, while the number of T$^{+}$ cells was considerably diminished (Fig. 6C, Figs. S3D,E and S5C, Table S3). RT-qPCR assays showed expression profiles similar to those obtained with LIF plus CHIR (Fig. 5I,J). Compared to protocol 8, cell aggregates supplemented only with low concentrations of BMP4, BMP8a, SCF and EGF showed that the generation of SSEA1$^{+}$-CD61$^{+}$ cells was reduced in *Otx2KO* cells and virtually absent in Δ*Obs* mutants (Fig. S6A,B). Therefore, data from protocols 7 and 8 indicate that in Δ*Obs* mutants, LIF addition to CHIR or to a minimal dosage of BMP4, BMP8a, SCF and EGF promotes efficient germline entry and severely affects somatic lineage. Based on these results, we asked whether combining LIF with CHIR and low

dosage of BMP4, BMP8a, SCF and EGF (protocol 9) could further augment PGCLC differentiation (Fig. 6F). Interestingly, the number of PGCLCs (Fig. 6G), the percentage of total cells expressing high OCT4, high NANOG, BLIMP1 and T (Fig. 6H, Figs. S3D,E and S5D, Table S3) and the expression profile exhibited by *Otx2*, *Oct4*, *Nanog*, *Ap2γ*, *Blimp1*, *T* and *Hoxb1* (Fig. 6I,J) were all similar to those obtained using the protocol 1. Furthermore, the level of H3K9me3 detected in *Oct4*Δ*Obs* cells was decreased on the DE and increased on the PE (Fig. 6K), suggesting that, as shown for protocol 1, OTX2 is required to prevent transition of the DE status from a poised to an active condition. To further assess the similarities between mature PGCLCs generated by protocols 1 and 9, expression of PGCLC-specific mRNAs was examined by RT-qPCR. SSEA1$^{+}$-CD61$^{+}$ cells purified at d6 using protocols 1 and 9 showed very similar expression of 11 PGCLC-specific mRNAs in both wt and mutant PGCLCs (Fig. S6C).Therefore, in Δ*Obs* mutants LIF, CHIR and low dosage of BMP4, BMP8a, SCF and EGF may cooperatively induce high levels of PGCLCs counterbalanced by severe decrease of somatic cells. Through this cooperation Δ*Obs* mutants exhibit close similarity with *Otx2KO* cells, a finding previously reported only for protocol 1. The significance of these data was reinforced by a further control experiment showing that in presence of CHIR and low dosage of BMP4, BMP8a, SCF and EGF, the generation of PGCLCs was considerably increased only in *Otx2KO* cells (Fig. S6D,E). To further investigate the role of LIF, the effect of titrating the LIF concentration on PGCLC differentiation was assessed. In GK15 media, the percentage of SSEA1$^{+}$-CD61$^{+}$ cells detected in wt cells was low but increased with increasing LIF concentrations, up to about 6% (Fig. S7A). In contrast, the mutant cell aggregates showed an increased yield of SSEA1$^{+}$-CD61$^{+}$ cells at 1000 U/ml LIF, compared to 300 U/ml, but this was not further increased by raising the LIF concentration to 3000 U/ml (protocol 4) (Fig. S7B). When a similar LIF titration was performed using the fixed concentrations of CHIR and low dosage of BMP4, BMP8a, SCF and EGF (protocol 9; Fig. S7C) a similar pattern of response was observed in both wt cells and in all mutant cell lines (Fig. S7D). While the absolute proportions of SSEA1$^{+}$-CD61$^{+}$ cells was increased in each cell line, the saturating response was seen in all the mutants to 1000 U/ml LIF but not in the wt cells (Fig. S7B), which at 3000 U/ml of LIF increased the percentage of PGCLCs up to 11%.

**Temporal expression changes during early PGCLC differentiation of Δ*Obs* mutants**

Previous data showed that the OTX2 repressive control of *Oct4* and *Nanog* expression defines commitment of EpiLC-derived cells to germline or somatic lineage. To deepen this aspect, we analyzed the combined expression of OTX2, OCT4, NANOG, SOX2, AP2γ and T in wt and Δ*Obs* cell aggregates at d0.5 and d1 using protocol 1. OCT4 and SOX2 were uniformly co-expressed in

wt and Δ*Obs* cells, while NANOG was detected mostly at low level in wt and at high level in Δ*Obs* cells (Fig. S8). Although, compared to EpiLCs, the *Otx2* mRNA was down-regulated at d0.5 and d1 (Fig. 2F), OTX2 was detectable in numerous cells co-expressing OCT4 and low NANOG in wt aggregates but co-expressing OCT4 and prevalently high NANOG in Δ*Obs* mutants (Fig. S8). All NANOG$^{+}$ cells co-expressed SOX2 (Fig. S8). In wt cells at d0.5 AP2γ was detected in very few OTX2$^{-}$ cells co-expressing high NANOG, while in Δ*Obs* mutants AP2γ was activated in a higher number of cells all co-expressing high NANOG and, frequently also OTX2 (Fig. S8), suggesting that in Δ*Obs* mutants numerous OTX2$^{+}$ cells are permissive for AP2γ activation. However, by d1 AP2γ co-expression with OTX2 was lost, likely for further down-regulation of OTX2 in AP2γ$^{+}$ cells. Analysis of T showed that at d1 in wt cells most of the OTX2$^{+}$ cells co-expressed T and low NANOG, while in Δ*Obs* mutants the few T$^{+}$ cells co-expressed only low NANOG (Fig. S8). These data suggest that OTX2-dependent, widespread activation of the pluripotency GRN determines in mutants a precocious and extensive recruitment of EpiLC-derived cells for germline entry rather than for somatic fate.

**The Obs2 in the *Oct4* enhancer plays a major role in germline and somatic differentiation**

To determine which Obs in the *Oct4* enhancer is functionally relevant, we restored in the *Oct4*Δ*Obs* mutant the wt sequence of Obs2, which exhibited the highest OTX2 binding activity, and generated the *Oct4*Δ*Obs1,3* ESC line (Fig. S1E,F). ChIP analysis showed the expected recovery in OTX2 binding specifically at Obs2 (Fig. S9A,B). FACS analysis showed that the percentage of PGCLCs generated by using protocol 1 was similar in wt and *Oct4*Δ*Obs1,3* mutant (Fig. S9C). Immunohistochemistry and cell counting at d2 (Figs. S9D,E and S3D,E; Table S2) confirmed the *Oct4*Δ*Obs1,3* similarity to wt cells, suggesting that OTX2 binding to Obs2 modulates the OCT4 requirement for germline and somatic differentiation.

**Enforced OTX2 expression inefficiently suppresses germline entry in Δ*Obs* mutants**

Previous work showed that Tamoxifen (Tx)-mediated nuclear translocation of OTX2-ER$^{T2}$ fusion protein in wt and *Otx2KO* cells suppresses PGCLC differentiation (Zhang et al., 2018). We reasoned that, in contrast to wt and *Otx2KO* cells, nuclear translocation of OTX2-ER$^{T2}$ in Δ*Obs* mutants should not affect functions depending on OTX2 binding to *Oct4* or *Nanog* enhancer region. To test this hypothesis, we generated *E14*;*Otx2ER*$^{T2}$, *Oct4*Δ*Obs*;*Otx2ER*$^{T2}$, *Nanog*Δ*Obs3;Otx2ER*$^{T2}$ and *Otx2KO;Otx2ER*$^{T2}$ ESC lines expressing similar level of OTX2-ER$^{T2}$ (Fig. S1G,H). In these

cell lines Tx exposure for 1 hour induced efficient OTX2-ER$^{T2}$ nuclear translocation (Fig. S1I). Two independent clones for *Oct4*Δ*Obs*;*Otx2ER*$^{T2}$ and *Nanog*Δ*Obs3;Otx2-ER*$^{T2}$ mutants were compared to *E14*;*Otx2ER*$^{T2}$ and *Otx2KO;Otx2ER*$^{T2}$ cell lines using protocol 1. Without Tx, the generation of PGCLCs was similar to that of the same parental cell lines (Fig. 7A). In Tx-treated cell aggregates (from d0 to d2 of the cell aggregation phase), the generation of PGCLCs was suppressed in *E14*;*Otx2ER*$^{T2}$ and *Otx2KO;Otx2ER*$^{T2}$ cell lines, severely affected in *Oct4*Δ*Obs*;*Otx2ER*$^{T2}$ cells, but only partially impaired in *Nanog*Δ*Obs3;Otx2ER*$^{T2}$ cells (Fig. 7B). Consistent with these findings, in Tx-treated d2 cell aggregates the generation of AP2γ$^{+}$-BLIMP1$^{+}$ cells was virtually abolished in *E14*;*Otx2ER*$^{T2}$ and *Otx2KO;Otx2ER*$^{T2}$ cells, decreased in *Oct4*Δ*Obs*;*Otx2ER*$^{T2}$ cells, but was less affected in *Nanog*Δ*Obs3;Otx2ER*$^{T2}$ cell aggregates (Fig. 7C). Conversely, the generation of T$^{+}$ cells was severely impaired only in *Nanog*Δ*Obs3;Otx2ER*$^{T2}$ cells (Fig. 7C). Interestingly, in *E14*;*Otx2ER*$^{T2}$, *Otx2KO;Otx2ER*$^{T2}$ and *Oct4*Δ*Obs*;*Otx2ER*$^{T2}$ cell lines, OCT4 expression was low in all cells including those AP2γ$^{+}$ (Fig. 7C), which did not activate NANOG and SOX2 (yellow and white arrows in Fig. 7C). In contrast, in *Nanog*Δ*Obs3;Otx2ER*$^{T2}$ mutant, a large fraction of AP2γ$^{+}$ cells showed high expression of OCT4 (pink arrows in Fig. 7C), NANOG and SOX2 (Fig. 7C). These data suggest that OTX2 binding to the *Nanog* enhancer is required to efficiently suppress germline differentiation and induce somatic fate. To investigate the possibility that OTX2 may repress germline determinants, we analyzed whether BLIMP1$^{+}$ cells co-expressed nuclear OTX2-ER$^{T2}$. BLIMP1 and OTX2-ER$^{T2}$ were co-localised in Tx-treated cells of all genotypes (Fig. 7D), which, in turn, also co-expressed AP2γ (Fig. 7C). In addition, we found that levels of *Prdm14* and *Blimp1* mRNAs, which are restricted to PGCLCs, showed a similar expression pattern in all cell lines (Fig. 7E). These data suggest that OTX2 does not directly repress *Blimp1*, *Ap2γ* and *Prdm14* during germline differentiation.

**Δ*Obs* embryos generate supernumerary PGCs**

To determine whether PGC development was affected also *in vivo*, we analysed Δ*Obs* homozygous embryos. Immunohistochemistry analysis at E6.7 and E7.5 revealed that expression of BLIMP1, AP2γ, FRAGILIS, NANOG, OCT4, T and OTX2 was similar to wt embryos (Fig. 8A). To determine the number of BLIMP1$^{+}$-FRAGILIS$^{+}$ PGCs we analyzed wt and Δ*Obs* embryos at E7.5 and E8.5. All sections including BLIMP1$^{+}$-FRAGILIS$^{+}$ PGCs were captured for cell counting (Fig. S10). Compared to wt, Δ*Obs* mutants exhibited about 1.5 times more PGCs at both E7.5 and E8.5 (Fig. 8B, Table S4). Ectopic PGCs were not identified. Therefore, binding of OTX2 to *Oct4* or *Nanog* enhancer region is required to limit the extent of germline differentiation *in vivo*.

## DISCUSSION

Differentiation of the epiblast into germline and somatic cells both *in vivo* and *in vitro* requires the action of BMP4, but the interplay with other signals, particularly WNT3, is also notable (Lawson et al., 1999; Saitou and Yamaji, 2012; Günesdogan and Surani, 2016; Aramaki et al., 2013). Previous studies have reported that LIF is required to sustain proliferation and survival of germ cells (Farini et al., 2005; Koshimizu et al., 1996; Cheng et al., 1994). The initial transition of epiblast-derived cells into the germline competent state requires dismantling of the formative pluripotency GRN, characterised by high *Otx2* expression and PE-driven expression of *Oct4*, alongside activation of the PGC pluripotency GRN, characterised by extinction of *Otx2*, re-expression of *Nanog*, high *Sox2* expression and DE-driven expression of *Oct4* (Zhang and Chambers, 2019; Smith, 2017; Choi et al., 2016). Conversely, somatic differentiation requires transition of formative pluripotency into a primed state characterized by cell heterogeneity in expression of pluripotency TFs including OTX2, NANOG and SOX2 as well as somatic gene expression.

Recent work has revealed that, in a germline permissive environment, down-regulation of *Otx2* determines the number of epiblast-derived cells entering the germline differentiation program (Zhang et al., 2018; Zhang and Chambers, 2019, Laird, 2018). Nevertheless, the mechanisms by which OTX2 regulates the contribution of epiblast cells to germline and somatic lineage are unknown. Since OTX2 binds to regulatory regions of *Oct4* and *Nanog* in EpiLCs (Acampora et al., 2016), we hypothesized that germline entry may require release of OTX2 repression on the PGCLC pluripotency GRN. Our data indicate that through this binding, OTX2 influences germline and somatic fate choice of EpiLC-derived cells in response to LIF and high dosage of BMP4, BMP8a, EGF and SCF. Indeed, Δ*Obs* and *Otx2KO* cell aggregates exhibit comparable phenotypes in terms of widespread activation of the pluripotency GRN, increased generation of PGCLCs and suppression of somatic fate. However, Δ*Obs* and *Otx2KO* mutants do not share all aspects of their phenotype in all protocols. Importantly, without cytokines, Δ*Obs* mutants, unlike *Otx2KO* cells (Zhang et al., 2018), do not generate PGCLCs. This suggests that OTX2 blocks cytokine-independent germline differentiation through functions other than those operating via binding to *Oct4* or *Nanog*. Such additional OTX2 functions could involve repression of PGCLC TFs. However, our evidence suggests that OTX2 does not directly repress *Blimp1*, *Prdm14* and *Ap2γ*.

To determine the signaling pathway modulations that may provide equally efficient PGCLC differentiation in Δ*Obs* and *Otx2KO* mutants, we analysed the effects of LIF, WNT or BMP4 alone (protocols 4-6). None of these protocols raises the efficiency of PGCLC generation by Δ*Obs* cells to the level achieved in *Otx2KO* mutants. However, the combined action of LIF, CHIR and a low dosage of BMP4, BMP8a, EGF and SCF suppresses the OTX2 functions that hamper

Δ*Obs* mutants from highly efficient, *Otx2KO*-like, germline entry to the same extent as in culture conditions with LIF and high dosage of BMP4, BMP8a, EGF and SCF. These data suggest that the generation of germ cells may be quantitatively correlated to specific combinations of cytokines whose inducing efficiency may be influenced also by the genetic state of the responding cells. In this context it would be interesting to assess whether in embryos the proximal-posterior epiblast includes restricted sub-domains where identity and fate of epiblast-derived cells are precisely regulated by different concentrations of LIF, BMP and WNT signaling molecules.

Together with dosage-dependent experiments (Fig. S7), our data indicate that LIF has an important role in PGCLC differentiation. We suggest that LIF signaling may improve the generation of PGCLCs by enhancing the proliferation/self-renewal of those cells that have released OTX2-dependent suppression of the pluripotency GRN. This interpretation may explain the beneficial effect of LIF on the generation of PGCLCs in all protocols where it is included, and, in addition, supports the similarity with ESCs where LIF is required to maintain pluripotency and self-renewal (Matsuda et al., 1999; Niwa et al., 2009), even through synergism with WNT and BMP4 signaling (ten Berge et al., 2011; Karwacki-Neisius et al., 2013; Ogawa et al., 2006; Ying et al., 2003, 2008). Notably, since *Otx2KO* ESCs can self-renew in the absence of LIF (Acampora et al., 2013), this might explain the propensity of *Otx2KO* ESCs to enter germline in the absence of LIF. We propose that in wt cells, LIF, BMP4 and WNT cooperate to repress *Otx2* early during the cell aggregation phase (Fig. 9). This generates two types of EpiLC-derived cells: those lacking OTX2 (OTX2$^-$) (right in Fig. 9A) and those transiently retaining OTX2 (OTX2$^+$) (left in Fig. 9A). OTX2$^-$ cells cannot repress the PGCLC pluripotency GRN, enter the unipotent germline state, are expanded by LIF or LIF in synergism with BMP4 and/or WNT and differentiate into PGCLCs (right in Fig. 9A). Conversely, OTX2-mediated repression of the PGCLC pluripotency GRN in OTX2$^+$ cells promotes entry into primed pluripotency and activation of somatic determinants leading to differentiation into somatic mesoderm (left in Fig. 9A). Our data do not exclude the possibility that BMP4 and WNT may also facilitate activation of somatic mesoderm genes (left in Fig. 9A). In Δ*Obs* mutants (Fig. 9B), *Otx2* repression by LIF, BMP4 and WNT and generation of OTX2$^-$ (right in Fig. 9B) and OTX2$^+$ (left in Fig. 9B) EpiLC-derived subtypes is comparable to wt cells. In Δ*Obs* mutants the OTX2$^-$ EpiLC-derived cell fraction corresponds to the wt OTX2$^-$ cell fraction, is naturally competent for germline differentiation and is unaffected by loss of OTX2 binding to *Oct4* or *Nanog* enhancer region (right in Fig. 9A,B). However, in the OTX2$^+$ cell fraction, progression towards the somatic fate is impaired by the inability of OTX2 to repress the pluripotency GRN (left in Fig. 9B). Consequently, cells that activate the pluripotency GRN may be further expanded by cytokines and commit to germline

entry. These early events result in an increased recruitment of EpiLC-derived cells for germline entry before somatic differentiation is initiated with a consequent switch from somatic to germline fate (Fig. 9B). According to this model, nuclear translocation of OTX2-ER$^{T2}$ can revert the germline to somatic fate switch in all cell lines except *Nanog*Δ*Obs3;Otx2ER*$^{T2}$ cells (Zhang et al., 2018), indicating that OTX2 binding to the *Nanog* enhancer region efficiently suppresses the PGCLC pluripotency GRN. Interestingly, compared to *Oct4*Δ*Obs;Otx2ER*$^{T2}$ cells, *Nanog*Δ*Obs3;Otx2ER*$^{T2}$ mutants produced a higher proportion of presumptive PGCLCs in the presence of Tx, indicating that OTX2 suppression of *Nanog* transcription may play a greater role in preventing PGCLC differentiation than suppression of *Oct4* transcription. A possible explanation may reside in the expression baseline exhibited by *Nanog* and *Oct4* in EpiLCs. Indeed for *Nanog*, transition from the EpiLC state to the cell-aggregation phase is accompanied by re-activation from a silent state while for *Oct4* this transition does not involve activation of expression, which is similar in EpiLCs and early EpiLC-derived cell aggregates, rather a change in its expression control from the PE to DE. Moreover, only in Tx-treated *Nanog*Δ*Obs3;Otx2ER*$^{T2}$ cells, activation of *Nanog* is accompanied by induction of *Sox2* in presumptive PGLCs suggesting that NANOG is required to induce *Sox2* and that both of them activate DE-driven expression of *Oct4* when OTX2 is suppressed. Notably, NANOG and SOX2 have been reported to bind to the DE of *Oct4* (Wu and Schöler, 2014). Importantly, this study shows that the repressive control exerted by OTX2 on *Oct4* or *Nanog* also occurs in Δ*Obs* homozygous embryos, which exhibit increased number of PGCs. Notably, PGC generation is not detected at ectopic sites in mutant embryos. This suggests that only proximal-posterior epiblast-derived cells, which lie close to the BMP4 source in the extraembryonic ectoderm, respond to loss of OTX2 binding to the *Oct4* or *Nanog* enhancer region by expanding generation of PGCs. However, our data do not currently distinguish between mechanisms involving a somatic mesoderm to germline fate switch of epiblast-derived cells or an alternative, cell-autonomous preferential proliferation of PGC precursors. In sum, previous work identified *Otx2* as a crucial determinant controlling allocation of epiblast cells to germline or somatic lineage (Zhang et al., 2018). Here we show that repression of *Oct4* and *Nanog* is a major mechanism by which OTX2 balances the contribution of epiblast cells to germline and somatic lineage, and, in addition, that OTX2 plays further roles preventing germline entry in the absence of cytokines.

## MATERIALS AND METHODS

### Generation of ESC and mouse mutants

Mutant ESC lines were generated by homologous recombination into E14Tg2a cells. The *Nanog*Δ*Obs3* ESC lines corresponding to clones 1 and 7, have previously been described (Acampora et al., 2016). In this study clone 1 was used for all experiments and clone 7 for independent confirmatory assays (Fig. 2). As for the *Oct4*Δ*Obs* ESC line, the mutant version of Obs1, Obs2 and Obs3 (Fig. S1A), was first introduced in the 5' flanking sequence of the *Oct4* gene by PCR-mediated mutagenesis, and then, this region was inserted into the targeting vector. Correct targeting into ESCs was assessed by Southern blot with probe a (Fig. S1B,C). Two *Oct4*Δ*Obs-neo/+* ESC clones were subjected to alternate rounds of neomycin cassette removal and re-targeting to obtain two independent homozygous ESC lines corresponding to clones 3 and 24 as confirmed by Southern blot and PCR analysis (Fig. S1C,D). Clone 24 represented an independent clone for confirmatory experiments (Fig. 2). The *Oct4*Δ*Obs* clone 3 was employed to perform all the experiments reported in this study. The *Oct4*Δ*Obs/+* ESC clone used to generate the *Oct4*Δ*Obs* clone 3, was also injected into C57BL/6 blastocysts to establish a mouse colony, which was kept into the B6D2 genetic background. *Oct4*Δ*Obs* homozygous mice were healthy and fertile. The homozygous *Oct4*Δ*Obs1,3* ESC line was also obtained by two alternate rounds of targeting and neomycin cassette removal in the homozygous *Oct4*Δ*Obs* cell line, by using a targeting vector carrying the mutant version of Obs1 and Obs3 sequences, but with the Obs2 sequence reverted to that of the wild type gene (Fig. S1E). Genotyping of the homozygous *Oct4*Δ*Obs1,3* cells was confirmed by PCR with allele-specific primers (Fig. S1F) and Southern blot (not shown). Primers for genotyping are listed in Table S5. The *pPyCAGOtx2-ER$^{T2}$* plasmid (Zhang et al., 2018) (Fig. S1G) was electroporated into E14, *Nanog*Δ*Obs3*, *Oct4*Δ*Obs*, and *Otx2KO* ESCs to generate cell lines showing cytoplasmic and ubiquitous distribution of the *OTX2-ER$^{T2}$* fusion protein whose nuclear translocation was dependent on 4-hydroxytamoxifen (Tx) (Sigma) administration. Twelve randomly integrated clones for each mutant cell line were assayed by Western blot to determine transgene expression. ESC lines exhibiting comparable levels of OTX2-ER$^{T2}$ were identified and those showing a level approximately twice that exhibited by the endogenous OTX2 were selected (Fig. S1H). These clones were then assayed by immunostaining with an antibody directed against ER. In the absence of Tx, the OTX2-ER$^{T2}$ protein was prevalently localized to the cytoplasm, whereas 1 hour of Tx (200 nM) exposure was sufficient to confine OTX2-ER$^{T2}$ to the nucleus (Fig. S1I).

All ESC lines of this study tested negative for mycoplasma contamination.

Experiments involving the use of animals were accomplished in accordance with the authorization n° 1196/2015-PR released by the Italian Ministry of Health.

**Cell culture experiments**

ESCs were either cultured in Glasgow Minimum Essential Medium (GMEM) medium (Sigma) supplemented with 12% FBS (HyClone) and 1,000U/ml of Leukemia Inhibitory Factor (LIF) (Millipore) (referred to as FBS+LIF), or in serum-free N2B27 medium (Gibco) supplemented with 500U/ml LIF, 1µM of the Mitogen-activated protein kinase kinase 1/2 (MEK1/2) inhibitor PD325901 (PD) and 3µM of the Glycogen synthase kinase 3 (GSK3) inhibitor CHIR99021 (CHIR) small molecules (both from Calbiochem) (referred to as LIF+2i) (Ying et al., 2008). Cell aggregates were generated from EpiLC induced from ESCs adapted to LIF+2i medium for a minimum of seven passages or maintained in FBS+LIF. ESCs ($2 \times 10^5$) were cultured in a 6-well plate coated with human fibronectin (Sigma) (16.7 µg/ml) in serum-free N2B27 medium containing 1% KnockOut Serum Replacement (KSR, Gibco ThermoFisher), 12 ng/ml of basic Fibroblast Growth Factor (FGF2) (PeproTech), and 20 ng/ml Activin A (R&D Systems) for 48 hours (Buecker et al., 2014). Then, EpiLCs were dissociated with TrypLE reagents (Gibco ThermoFisher) and resuspended at a concentration of $8 \times 10^4$ cells/ml in GMEM medium containing 15% KSR (GK15) or together with various combinations of cytokines and small molecules. Next, 25µl of cell suspension (about 2000 cells) was plated on the lids of tissue culture dishes and incubated, as hanging drops, over PBS-containing bottom plates. After two days, cell aggregates were either collected for immunohistochemistry on sections and cytospin experiments, or transferred to ultralow adhesion 24-well plates (Corning) where they were incubated in the same culture media for additional four days before FACS analysis. Medium was replaced every other day. Culture conditions for cell aggregates were based on the method reported by Hayashi et al. (Hayashi et al., 2011).

In protocol 1 cell aggregates were cultured in GK15 supplemented with LIF (1,000 U/ml), Bone Morphogenetic Protein 4 (BMP4) (50 ng/ml), BMP8a (50 ng/ml), Stem Cell Factor (SCF) (10 ng/ml) (all from R&D Systems), Epidermal Growth Factor (EGF) (10 ng/ml) (PeproTech) (Zhang et al., 2018; Hayashi et al., 2011) (Figs. 1B and 2A). Protocol 2 differed from protocol 1 only for ESCs that were maintained in FBS+LIF (Fig. 2I). In protocol 3 cell aggregates were cultured only in GK15 medium (Fig. 3A). In protocol 4 cell aggregates were cultured in GK15 with LIF (1000U/ml) only (Fig. 4A). In protocol 5 cell aggregates were cultured in GK15 supplemented with

BMP4 (50 ng/ml), BMP8a (50 ng/ml), SCF (10 ng/ml), EGF (10 ng/ml) and without LIF (Fig. 4F). In protocol 6 cell aggregates were cultured in GK15 supplemented with CHIR (3µM) only (Fig. 5A). In protocol 7 cell aggregates were cultured in GK15 supplemented with LIF (1,000 U/ml) and CHIR (3µM) (Fig. 5F). In protocol 8 cell aggregates were cultured in GK15 supplemented with LIF (1,000U/ml) and low dosage of BMP4 (5ng/ml), BMP8a (5ng/ml), SCF (1ng/ml) and EGF (1ng/ml) (Fig. 6A). In protocol 9 cell aggregates were cultured in GK15 supplemented with LIF (1,000U/ml), CHIR (3µM) and low dosage of BMP4 (5ng/ml), BMP8a (5ng/ml), SCF (1ng/ml) and EGF (1ng/ml) (Fig. 6F).

Two additional culture conditions without LIF were employed as control experiments: in the first condition, cell aggregates were cultured in GK15 supplemented with low dosage of BMP4 (5ng/ml), BMP8a (5ng/ml), SCF (1ng/ml) and EGF (1ng/ml) (Fig. S6A); in the second condition cell aggregates were cultured in GK15 supplemented with CHIR (3µM) and low dosage of BMP4 (5ng/ml), BMP8a (5ng/ml), SCF (1ng/ml) and EGF (1ng/ml) (Fig. S6D).

For experiments performed to assess the effect of different concentrations of LIF, wt and mutant cell aggregates were cultured according to the standard and modified versions of protocols 4 and 9. For protocol 4, cell aggregates were cultured for 6 days in GK15 medium supplemented with 300, 1000 (standard protocol 4) and 3000 U/ml of LIF only (Fig. S7A,B); for protocol 9 cell aggregates were cultured in the presence of fixed concentrations of CHIR (3µM) and low dosage of BMP4 (5ng/ml), BMP8a (5ng/ml), SCF (1ng/ml) and EGF (1ng/ml) in combination with 300, 1000 (standard protocol 9) and 3000 U/ml of LIF (Fig. S7C,D).

For experiments involving *E14*;*Otx2ER*$^{T2}$, *Oct4*Δ*Obs*;*Otx2ER*$^{T2}$, *Nanog*Δ*Obs3;Otx2ER*$^{T2}$ and *Otx2KO;Otx2ER*$^{T2}$ cell lines, Tx (200nM) was administered from d0 to d2 of the cell aggregation phase both for FACS experiments on d6 and immunohistochemistry and RT-qPCR analyses on d2. For these cell lines EpiLC-derived cell aggregates were cultured following protocol 1 conditions.

**Alkaline phosphatase (ALP) assay, FGF2 and LIF response experiments**

For ALP staining, $8x10^2$ ESCs cultured in FBS+LIF medium were seeded as triplicates in 6-well plates and grown for 5 days. Upon fixation into 10% Neutral Buffered Formalin (Sigma), ALP activity was revealed by 30 minutes incubation into a freshly made solution containing 0.1 M Tris-HCl (pH 8.3), Naphthol AS MX-$PO_4$ (5 mg, pre-dissolved in 200µl of N,N-Dimethylformamide,) as phosphatase substrate, and Fast Red Violet (30 mg) as dye (both from Sigma) in a 50 ml final volume. After a few washes in water, colonies were scored for those exhibiting homogeneous staining and counted. For LIF response experiments, ESCs were kept for up to 1 hour in GMEM containing 15% KSR in the absence of LIF, which was then added back to the medium at a

concentration of $10^3$ Units /ml. p-STAT3 was monitored after 20 minutes by Western blots (Acampora et al., 2017). For FGF2 response, ESCs were washed and kept in GMEM containing 5% KSR with or without FGF2 at a concentration of 5 ng/ml for 15 and 45 minutes (Acampora et al., 2016). FGF2 response was determined by assessing the level of p-ERK1,2 in Western blots.

**ChIP experiments**

ChIP experiments were performed as previously described (Lee et al., 2006) on wt and *Otx2KO* ESCs and EpiLCs with a rabbit polyclonal OTX2 antibody (Acampora et al., 2016), and on d2 cell aggregates with a rabbit histone H3 tri-methyl lysine 9 (H3K9me3) antibody and normal rabbit IgG. On the day before chromatin preparation, Dynabeads Protein A (Invitrogen) were washed three times with PBS containing 0.5% BSA and pre-adsorbed over-night with the different antibodies and normal rabbit IgG. Only for aggregates, cells were washed with PBS and trypsinized before fixation. Then, formaldehyde (1%) cross-linked cells were quenched with 125 mM glycine and washed twice with cold PBS. Upon collection and centrifugation at 4°C, cells were lysed in LB1 buffer (50 mM Hepes-KOH, 140 mM NaCl, 1 mM EDTA, 10% glycerol, 0.5% NP-40, 0.25% Triton X-100), then were resuspended in LB2 buffer (10 mM Tris-HCl pH 8.0, 200 mM NaCl, 1 mM EDTA, 0.5 mM EGTA), rocking at 4°C for 10 min each time. Isolated nuclei were resuspended into LB3 buffer (10 mM Tris-HCl pH 8, 100mM NaCl, 1mM EDTA, 0.5 mM EGTA, 0.1% Na-Deoxycholate, 0.5% N-lauroylsarcosine Na-salt) and kept on ice. All lysis buffers were prepared with freshly added protease inhibitor cocktail plus PMSF. Sonication was performed with a Misonix 2000 sonicator to obtain fragment size with a peak of approximately 500 base pairs or 300 base pairs respectively for OTX2 or H3K9me3 ChIP assays. SDS 0.1%, (only for OTX2 ChIP assays) and Triton X-100 (1%) were added to sonicated chromatin before centrifugation to remove debris. Supernatant was then incubated with the antibody- or IgG-coated beads on a rotator at 4°C for at least 18 hours (Acampora et al., 2016). Beads were collected at any step through the magnetic stand and sequentially washed with low-salt solution (0.1% SDS, 1% Triton, 2 mM EDTA pH8, 20 mM Tris-HCl pH 8, 150 mM NaCl), high-salt solution (0.1% SDS, 1% Triton, 2mM EDTA, 20mM Tris-HCl pH 8, 500 mM NaCl), LiCl solution (0.25 M LiCl, 1% NP40, 1% Na-Deoxycholate, 10 mM Tris-HCl pH 8), and TE buffer (Tris-HCl 10mM pH 8, 1 mM EDTA) containing 50 mM NaCl. Beads were then incubated for 15 min at 65°C with elution buffer (50 mM Tris-HCl pH 8, 10 mM EDTA, 1% SDS). The immunoprecipitated DNA (IP) was separated from the beads and reverse crosslinked along with input (non-IP DNA) by overnight incubation at 65°C. After RNA and protein digestion, DNA samples were purified by Phenol-Chloroform extraction and Ethanol precipitation. DNA was resuspended in 10 mM Tris-HCl pH 8 and used in standard qPCR reactions. Fold enrichment of

OTX2 ChIP samples was calculated relative to ChIP in *Otx2KO* cells, used as negative control, according to the $2^{-\Delta\Delta Ct}$ formula. ChIP values for H3K9me3 and control IgG were calculated as percent of input, according to the formula: % Input $=2^{-\Delta Ct(\text{normalized ChIP})}$. Data are represented as mean ± standard deviation (SD) of three independent experiments, each in technical triplicates. ChIP primers are listed in Table S5.

**Immunocytochemistry and immunohistochemistry**

For immunocytochemistry experiments on ESCs and EpiLCs, adherent cells grown on 4-well chamber slides (Sarstedt) were PBS washed and fixed with 4% paraformaldehyde (PFA). Blocking (1 hour) and incubation with primary antibodies (overnight) were performed in PBS containing 0,3% triton X-100 and 2% skimmed milk powder (BioRad). Cells were washed three times with PBS before and after incubation with Alexa fluor secondary antibodies (90 min). Cells were then counterstained with Dapi (Acampora et al., 2016). Immunohistochemistry experiments on d2 PGCLCs were performed on an average of 100-150 cell aggregates per experiment. After washing in PBS, cell aggregates were fixed overnight in 4% PFA, then dehydrated and processed for paraffin embedding and microtome sectioning. Slides were then xylene-deparaffinized and rehydrated through a descending series of alcohol to water before been boiled into citrate buffer pH 6.0 for antigen retrieval. Sections were then incubated with a blocking solution containing 0.5% milk, 10% FBS, 1% BSA and hybridized with the primary and Alexa fluor secondary antibodies as described before. (Acampora et al., 2013). For immunostaining of cytospin preparations, d2 cell aggregates were collected, washed twice with PBS, dissociated with trypsin and resuspended in 5% FBS in PBS to obtain a single cell suspension. After centrifugation, cells were resuspended at $1x10^6$ cells/ml in 1% BSA in PBS and $2x10^5$ cells were loaded onto cytofunnels and centrifuged for 7 min at 1000 r.p.m. Cells were fixed in 4% PFA and processed for immunostaining as described for ESCs and EpiLCs.

For *in vivo* PGC counting, embryos obtained from natural matings of age-matched (3 month-old), randomly selected breeding pairs of wild type and Δ*Obs* mutants were collected at E7.5 and E8.5, fixed overnight in 4% PFA in PBS, dehydrated, paraffin embedded and sectioned. Embryos matched for morphology or number of somites, were processed for immunostaining with FRAGILIS and BLIMP1 antibodies as for cell aggregates. All sections including PGCs were selected and captured for cell counting. All immunostaining images were captured with a Nikon eclipse NI microscope. For immunohistochemistry experiments performed with 3 compatible antibodies, fluorescence was excited at 405 nm for Dapi and at 488 nm, 555 nm and 647 nm for secondary antibodies. Eventually, red color for fluorescence excited at 555 nm was converted to

green pseudocolor to allow merging of all combinations. All antibodies employed for immunostaining experiments are listed in Table S6.

**Cell counting and statistical analysis**

Cytospin assays were immunostained and 3 non-overlapping fields per experiment were captured, images were printed in A4 format and cell number manually determined. Standard deviation (SD) was calculated from the analysis of three independent experiments for each differentiation protocol and for each cell line (Tables S2 and S3). Similarly, also for PGC counting in embryos, immunostained sections were selected, captured, printed in A4 format and FRAGILIS$^{+}$- BLIMP1$^{+}$ cells counted. Embryos were selected by morphology at E7.5 and by morphology and number of somites at E8.5. SD was determined by the analysis of 6 and 7 embryos/genotype respectively at E7.5 and E8.5 (Table S4). *P* value was determined by using the one-tail or two tails Student *t* test.

**Flow cytometry**

FACS analysis was performed on d6 cell aggregates. An average of 50-60 aggregates were collected and dissociated into single cells with trypsin and neutralized in PBS containing 10% FBS. A maximum of 5 x $10^5$ cells were collected by centrifugation and the pellet resuspended in 100µl PBS plus 10% FBS supplemented with Alexa Fluor 647 anti-mouse/human CD15 (SSEA1) (Biolegend) and PE anti mouse/rat CD61 (Biolegend) (Zhang et al., 2018), diluted 1/200 and 1/500, respectively, and incubated for 30 min at 4 °C. Cells were washed twice in 1 ml PBS plus 10% FBS before analysis on a BD FACSAria III (Becton Dickinson). Data were acquired using BD FACSDiva software 8.0.1 and analyzed using FlowJo software version 10.7.1. Gating strategy is shown in Fig. S3A. The dissociated cell population was first gated on the basis of the FSC (size) and SSC (complexities) scatter plot; singlets were then selected based on the linear correlation between the FSC-area (FSC-A) and the FSC-height (FSC-H); dead cells were excluded by 7-AAD dye (Fig. S3A-C). All FACS assays were performed in at least three independent experiments.

**Chimerism assay**

c57BL/6 blastocysts were injected with *Oct4ΔObs* ESCs (n=10 cells/embryo), for a total of 50 embryos and transferred into B6D2F1 foster mothers. Chimerism was assessed by extent of coat color mosaicism.

**RNA extraction, cDNA synthesis and RT-qPCR experiments**

Total RNA was extracted from cell lysates using TRIzol® Reagent (Invitrogen) and reverse transcribed using Superscript II (Invitrogen) according to the manufacturer's instructions. First-strand cDNA was used for RT-qPCR analysis using Power SYBR Green Master Mix (Applied Biosystems). RT-qPCR experiments were performed on RNA extracted from about 80 cell aggregates per time point (from EpiLC, throughout day 2) for protocols 1, 3-9, using primers specific for *Otx2*, *Oct4*, *Nanog*, *Ap2γ*, *Blimp1*, *T* and *Hoxb1*. RT-qPCR experiments were also performed on RNA extracted from SSEA1$^{+}$-CD61$^{+}$ cells, FACS-sorted with the same gating strategy previously described, at day 6 of PGCLC differentiation using protocols 1 and 9. For SSEA1$^{+}$-CD61$^{+}$ sorted cells, primers were specific for *Blimp1*, *Prdm14*, *Ap2γ*, *Nanos3*, *Ddx4* (also known as *Mvh*), *Prmt5*, *Fragilis*, *ALPL* (also known as *TNAP*), *Gcna1*, *DAZL* (also known as *DAZLA),* and *Kit*. Gene expression was normalized to *TATA-box Binding Protein* (*TBP*) transcripts according to $2^{(Ct\ TBP\ -\ Ct\ target)}$ formula. Experiments were performed as biological triplicates and technical duplicates. Oligonucleotide sequences for RT-qPCR analysis are listed in Table S5.

**Western blot assay**

Total cell lysates were loaded and run on a 10.5% SDS-PAGE gel. Proteins were transferred onto Protran nitrocellulose membranes (GE Healthcare), blocked in 5% skimmed milk (BioRad) for 1 hour at room temperature, and incubated with primary antibodies (4°C, overnight). PBS plus Tween 20 washes were carried out before and after secondary antibodies incubation (1 hour at room temperature). Protein expression was revealed by ECL reactions (GE Healthcare). Western Blot antibodies are listed in Table S6.

**Acknowledgments**

We thank members of the I.C. lab and V. Wilson for comments on the manuscript, L. Pisapia for support in FACS data analysis, the staff of the IGB animal house and that of the IGB FACS facility. We also thank D. Graniero for typing and formatting the manuscript.

**Competing interests**

The authors declare no competing interest.

**Author contributions**

L.G.D.G. and D.A. designed the experiments with A.S. and performed most of them. D.O. contributed to the experiments on OTX2 over-expressing cell lines. V.N. contributed to the analysis of data. P.B. performed with D.A. FACS analysis. E.B. contributed to the analysis of data. I.C. contributed to the analysis of data and the preparation of manuscript. A.S. supervised the study and wrote the manuscript with the input of I.C. and D.A.

**Funding**

This work was supported by the project SATIN-POR CAMPANIA FESR 2014/2020, and the PRIN project from MIUR (20157JF8P5_004) to A.S. and by the Medical Research Council (UK) grant MR/T003162/1 to I.C.; E.B. is supported by a Marie Sklodowska-Curie fellowship (H2020-MSCA-IF-2018/843879).

## REFERENCES


**Acampora, D. Mazan, S., Lallemand, Y., Avantaggiato, V., Maury, M., Simeone, A. and Brûlet, P**. (1995). Forebrain and midbrain regions are deleted in Otx2-/- mutants due to a defective anterior neuroectoderm specification during gastrulation. *Development* **121**, 3279-3290.

**Acampora, D., Omodei, D., Petrosino, G., Garofalo, A., Savarese, M., Nigro, V., Di Giovannantonio, L. G., Mercadante, V. and Simeone, A.** (2016). Loss of the Otx2 binding site in the Nanog promoter affects the integrity of embryonic stem cell subtypes and specification of inner cell mass-derived epiblast. *Cell Rep*. **15**, 2651-2664.

**Acampora, D., Di Giovannantonio, L. G. and Simeone, A**. (2013). Otx2 is an intrinsic determinant of the embryonic stem cell state and is required for transition to a stable epiblast stem cell condition. *Development* **140**, 43-55.

**Acampora, D., Di Giovannantonio, L. G., Garofalo, A., Nigro, V., Omodei, D., Lombardi, A., Zhang, J., Chambers, I. and Simeone, A.** (2017). Functional antagonism between OTX2 and NANOG specifies a spectrum of heterogeneous identities in embryonic stem cells. *Stem Cell Reports* **9**,1642-1659.

**Ancelin, K., Lange, U. C., Hajkova, P., Schneider, R., Bannister, A. J., Kouzarides, T. and Surani, M. A.** (2006). Blimp1 associates with Prmt5 and directs histone arginine methylation in mouse germ cells. *Nat. Cell Biol.* **8**, 623-630.

**Aramaki, S., Hayashi, K., Kurimoto, K., Ohta, H., Yabuta, Y., Iwanari, H., Mochizuki, Y., Hamakubo, T., Kato, Y., Shirahige, K. et al.** (2013). A mesodermal factor, T, specifies mouse germ cell fate by directly activating germline determinants. *Dev. Cell* **27**, 516-529.

**Buecker, C., Srinivasan, R., Wu, Z., Calo, E., Acampora, D., Faial, T., Simeone, A., Tan, M., Swigut, T. and Wysocka, J.** (2014). Reorganization of enhancer patterns in transition from naive to primed pluripotency. *Cell Stem Cell* **14**, 838-853.

**Campolo, F., Gori, M., Favaro, R., Nicolis, S., Pellegrini, M., Botti, F., Rossi, P., Jannini, E. A. and Dolci, S.** (2013). Essential role of Sox2 for the establishment and maintenance of the germ cell line. *Stem Cells* **31**, 1408-1421.

**Chambers, I., Silva, J., Colby, D., Nichols, J., Nijmeijer, B., Robertson, M., Vrana, J., Jones, K., Grotewold, L. and Smith, A.** (2007). Nanog safeguards pluripotency and mediates germline development. *Nature* **450**, 1230-1234.

**Cheng, L., Gearing, D. P., White, L. S., Compton, D. L., Schooley, K. and Donovan, P. J.** (1994). Role of leukemia inhibitory factor and its receptor in mouse primordial germ cell growth. *Development* **120**, 3145-3153.

**Choi, H. W., Joo, J.Y., Hong, Y. J., Kim, J. S., Song, H., Lee, J. W., Wu, G., Schöler, H. R. and Do, J. T.** (2016). Distinct enhancer activity of Oct4 in naive and primed mouse pluripotency. *Stem Cell Reports* **7**, 911-926.

**Farini, D., Scaldaferri, M. L., Iona, S., La Sala, G. and De Felici, M.** (2005). Growth factors sustain primordial germ cell survival, proliferation and entering into meiosis in the absence of somatic cells. *Dev. Biol.* **285**, 49-56.

**Günesdogan, U. and Surani, M. A.** (2016). Developmental competence for primordial germ cell fate. *Curr. Top. Dev. Biol.* **117**, 471-496.

**Hackett, J.A. and Surani, M. A**. (2014). Regulatory principles of pluripotency: from the ground state up. *Cell Stem Cell* **15**, 416-430.

**Hayashi, K., Ogushi, S., Kurimoto, K., Shimamoto, S., Ohta, H. and Saitou, M.** (2012). Offspring from oocytes derived from in vitro primordial germ cell-like cells in mice. *Science* **338**, 971-975.

**Hayashi, K., de Sousa Lopes, S. M. and Surani, M. A**. (2007). Germ cell specification in mice. *Science* **316**, 394-396.

**Hayashi, K., Ohta, H., Kurimoto, K., Aramaki, S. and Saitou, M.** (2011). Reconstitution of the mouse germ cell specification pathway in culture by pluripotent stem cells. *Cell* **146**, 519-532.

**Hayashi, M., Kawaguchi, T., Durcova-Hills, G. and Imai, H.** (2017). Generation of germ cells from pluripotent stem cells in mammals. *Reprod. Med. Biol*. **17**, 107-114.

**Johnson, A. D. and Alberio, R.** (2015). Primordial germ cells: the first cell lineage or the last cells standing? *Development* **142**, 2730-2739.

**Johnson, A. D., Crother, B., White, M. E., Patient, R., Bachvarova, R. F., Drum, M. and Masi, T.** (2003). Regulative germ cell specification in axolotl embryos: a primitive trait conserved in the mammalian lineage. *Philos. Trans. R. Soc. Lond. B. Biol. Sci.* **358**, 1371-1379.

**Karwacki-Neisius, V., Göke, J., Osorno, R., Halbritter, F., Ng, J. H., Weiße, A. Y., Wong, F. C., Gagliardi, A., Mullin, N. P., Festuccia, N., et al.** (2013). Reduced Oct4 expression directs a robust pluripotent state with distinct signaling activity and increased enhancer occupancy by Oct4 and Nanog. *Cell Stem Cell* **12**, 531-545.

**Kehler, J., Tolkunova, E., Koschorz, B., Pesce, M., Gentile, L., Boiani, M., Lomelí, H., Nagy, A., McLaughlin, K. J., Schöler, H. R et al**. (2004). Oct4 is required for primordial germ cell survival. *EMBO Rep.* **5**, 1078-1083.

**Koshimizu, U., Taga, T., Watanabe, M., Saito, M., Shirayoshi, Y., Kishimoto, T. and Nakatsuji, N.** (1996). Functional requirement of gp130-mediated signaling for growth and survival of mouse primordial germ cells in vitro and derivation of embryonic germ (EG) cells. *Development* **122**, 1235-1242.

**Kurimoto, K., Yabuta, Y., Ohinata, Y., Shigeta, M., Yamanaka, K. and Saitou, M.** (2008). Complex genome-wide transcription dynamics orchestrated by Blimp1 for the specification of the germ cell lineage in mice. *Genes Dev.* **22**, 1617-1635.

**Laird, D. J.** (2018). How to lose your inheritance. *Nature* **562**, 497-498.

**Lawson, K. A., Dunn, N. R., Roelen, B. A., Zeinstra, L. M., Davis, A. M., Wright, C. V., Korving, J. P. and Hogan, B. L.** (1999). Bmp4 is required for the generation of primordial germ cells in the mouse embryo. *Genes Dev.* **13**, 424-436.

**Lee, T.I., Johnstone, S.E. and Young, R.A.** (2006). Chromatin immunoprecipitation and microarray-based analysis of protein location. *Nat. Protoc.* **1**, 729-748.

**Leitch, H. G., Nichols, J., Humphreys, P., Mulas, C., Martello, G., Lee, C., Jones, K., Surani, M. A. and Smith A**. (2013). Rebuilding pluripotency from primordial germ cells. *Stem Cell Reports* **1**, 66-78.

**Magnúsdóttir, E., Dietmann, S., Murakami, K., Günesdogan, U., Tang, F., Bao, S., Diamanti, E., Lao, K., Gottgens, B. and Azim Surani, M.** (2013). A tripartite transcription factor network regulates primordial germ cell specification in mice. *Nat. Cell Biol.* **15**, 905-915.

**Matsuda, T., Nakamura, T., Nakao, K., Arai, T., Katsuki, M., Heike, T. and Yokota, T.** (1999). STAT3 Activation is sufficient to maintain an undifferentiated state of mouse embryonic stem cells. *EMBO J.* **18**, 4261-4269.

**Murakami, K., Günesdogan, U., Zylicz, J. J., Tang, W. W. C., Sengupta, R., Kobayashi, T., Kim, S., Butler, R., Dietmann, S. and Surani, M. A.** (2016). NANOG alone induces germ cells in primed epiblast in vitro by activation of enhancers. *Nature* **529**, 403-407.

**Nakaki, F., Hayashi, K., Ohta, H., Kurimoto, K., Yabuta, Y. and Saitou, M.** (2013). Induction of mouse germ-cell fate by transcription factors in vitro. *Nature* **501**, 222-226.

**Neagu, A., van Genderen, E., Escudero, I., Verwegen, L., Kurek, D., Lehmann, J., Stel, J., Dirks, R. A. M., van Mierlo, G., Maas, A. et al.** (2020). In vitro capture and characterization of embryonic rosette-stage pluripotency between naive and primed states. *Nat. Cell Biol.* **22**, 534-545.

**Niwa, H., Ogawa, K., Shimosato, D. and Adachi, K.** (2009). A parallel circuit of LIF signaling pathways maintains pluripotency of mouse ES cells. *Nature* **460**, 118-122.

**Ogawa, K., Nishinakamura, R., Iwamatsu, Y., Shimosato, D. and Niwa, H.** (2006). Synergistic action of Wnt and LIF in maintaining pluripotency of mouse ES cells. *Biochem. Biophys. Res. Commun.* **343**, 159-166.

**Ohinata, Y., Payer, B., O'Carroll, D., Ancelin, K., Ono, Y., Sano, M., Barton, S. C., Obukhanych, T., Nussenzweig, M., Tarakhovsky, A., et al.** (2005). Blimp1 is a critical determinant of the germ cell lineage in mice. *Nature* **436**, 207-213.

**Ohinata, Y., Ohta, H., Shigeta, M., Yamanaka, K., Wakayama, T. and Saitou, M.** (2009). A signaling principle for the specification of the germ cell lineage in mice. *Cell* **137**, 571-584.

**Okamura, D., Tokitake, Y., Niwa, H. and Matsui, Y.** (2008). Requirement of Oct3/4 function for germ cell specification. *Dev. Biol.* **317**, 576-584.

**Saitou, M.** (2009). Germ cell specification in mice. *Curr. Opin. Genet. Dev.* **19**, 386-395.

**Saitou, M. and Yamaji, M**. (2012). Primordial germ cells in mice. *Cold Spring Harb. Perspect. Biol.* **4**, 1-19.

**Saitou, M., Barton, S. C. and Surani M. A.** (2002). A molecular programme for the specification of germ cell fate in mice. *Nature* **418**, 293-300.

**Saitou, M., Payer, B., O'Carroll, D., Ohinata, Y. and Surani, M. A.** (2005). Blimp1 and the emergence of the germ line during development in the mouse. *Cell Cycle* **4**, 1736-1740.

**Senft, A.D., Bikoff, E. K., Robertson, E. J. and Costello, I.** (2019). Genetic dissection of Nodal and Bmp signaling requirements during primordial germ cell development in mouse. *Nat. Commun.* **10**, 1-11.

**Smith, A.** (2017). Formative pluripotency: the executive phase in a developmental continuum. *Development* **144**, 365-373.

**Surani, M. A**. (2001). Reprogramming of genome function through epigenetic inheritance. *Nature* **414**, 122-128.

**Surani, M. A., Hayashi, K. and Hajkova, P.** (2007). Genetic and epigenetic regulators of pluripotency. *Cell* **128**, 747-762.

**ten Berge, D., Kurek, D., Blauwkamp, T., Koole, W., Maas, A., Eroglu, E., Siu, R. K. and Nusse, R.** (2011). Embryonic Stem Cells Require Wnt Proteins to Prevent Differentiation to Epiblast Stem Cells. *Nat. Cell. Biol.* **13**, 1070-1075.

**Vincent, S. D., Dunn, N. R., Sciammas, R., Shapiro-Shalef, M., Davis, M. M., Calame, K., Bikoff, E. K. and Robertson, E. J.** (2005). The zinc finger transcriptional repressor Blimp1/Prdm1 is dispensable for early axis formation but is required for specification of primordial germ cells in the mouse. *Development* **132**, 1315-1325.

**Weber, S., Eckert, D., Nettersheim, D., Gillis, A. J. M., Schäfer, S., Kuckenberg, P., Ehlermann, J., Werling, U., Biermann, K., , L. H. J. et al.** (2010). Critical function of AP-2 gamma/TCFAP2C in mouse embryonic germ cell maintenance. *Biol. Reprod.* **82**, 214-223 (2010).

**Wu, G. and Schöler, H. R.** (2014). Role of Oct4 in the early embryo development. *Cell. Regen.* **3**, 3-7.

**Wylie, C.** (1999). Germ cells. *Cell* **96**, 165-174.

**Yamaguchi, S., Kurimoto, K., Yabuta, Y., Sasaki, H., Nakatsuji, N., Saitou, M. and Tada, T.** (2009). Conditional knockdown of Nanog induces apoptotic cell death in mouse migrating primordial germ cells. *Development* **136**, 4011-4020.

**Yamaji, M., Seki, Y., Kurimoto, K., Yabuta, Y., Yuasa, M., Shigeta, M., Yamanaka, K., Ohinata, Y. and Saitou, M.** (2008). Critical function of Prdm14 for the establishment of the germ cell lineage in mice. *Nat. Genet*. **40**, 1016-1022.

**Yang, S. H., Kalkan, T., Morissroe, C., Marks, H., Stunnenberg, H., Smith, A. and Sharrocks, A. D.** (2014). Otx2 and Oct4 drive early enhancer activation during embryonic stem cell transition from naive pluripotency. *Cell Rep.* **7**, 1968-1981.

**Yeom, Y. I., Fuhrmann, G., Ovitt, C. E., Brehm, A., Ohbo, K., Gross, M., Hübner, K. and Schöler, H. R.** (1996). Germline regulatory element of Oct-4 specific for the totipotent cycle of embryonal cells. *Development* **122**, 881-894.

**Ying, Q. L., Wray, J., Nichols, J., Batlle-Morera, L., Doble, B., Woodgett, J., Cohen, P. and Smith, A.** (2008). The ground state of embryonic stem cell self-renewal. Nature **453**, 519-523.

**Ying, Q. L., Nichols, J., Chambers, I. and Smith, A.** (2003). BMP induction of Id proteins suppresses differentiation and sustains embryonic stem cell self-renewal in collaboration with STAT3. *Cell* **115**, 281-292.

**Zhang, J., Zhang, M., Acampora, D., Vojtek, M., Yuan, D., Simeone, A and Chambers, I.** (2018). OTX2 restricts entry to the mouse germline. *Nature* **562**, 595-599.

**Zhang, M. and Chambers, I.** (2019). Segregation of the mouse germline and soma. *Cell Cycle* **18**, 3064-3071.

## Figures

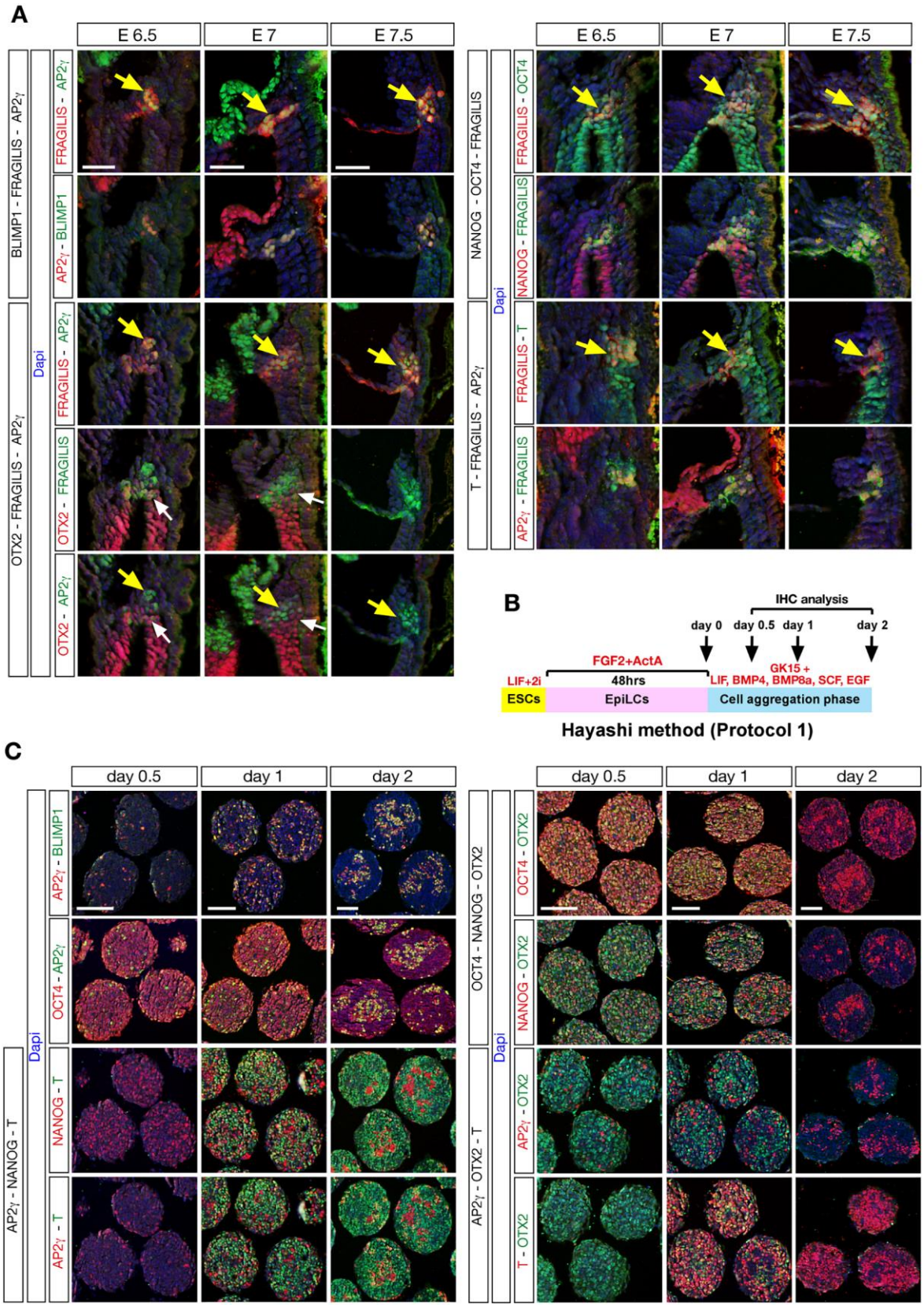

**Fig. 1. Expression analysis during germline differentiation.** (A) Representative sections of E6.5, E7 and E7.5 embryos stained with the indicated antibody combinations. Yellow arrows, differentiating PGCs; white arrows, FRAGILIS$^{+}$-AP2$\gamma^{-}$ cells with low or moderate OTX2 levels. Note that at E6.5 sections are along a sagittal-oblique plane and at E7 and E7.5 sections are along a sagittal plane. Scale bar = 50µm. (B) Protocol 1 experimental design. Cell aggregates were analyzed at d0.5, d1 and d2. (C) Immunohistochemistry analysis performed on representative sections using the indicated antibody combinations.. Scale bar = 100µm. (A,C) Sections were counterstained with Dapi.

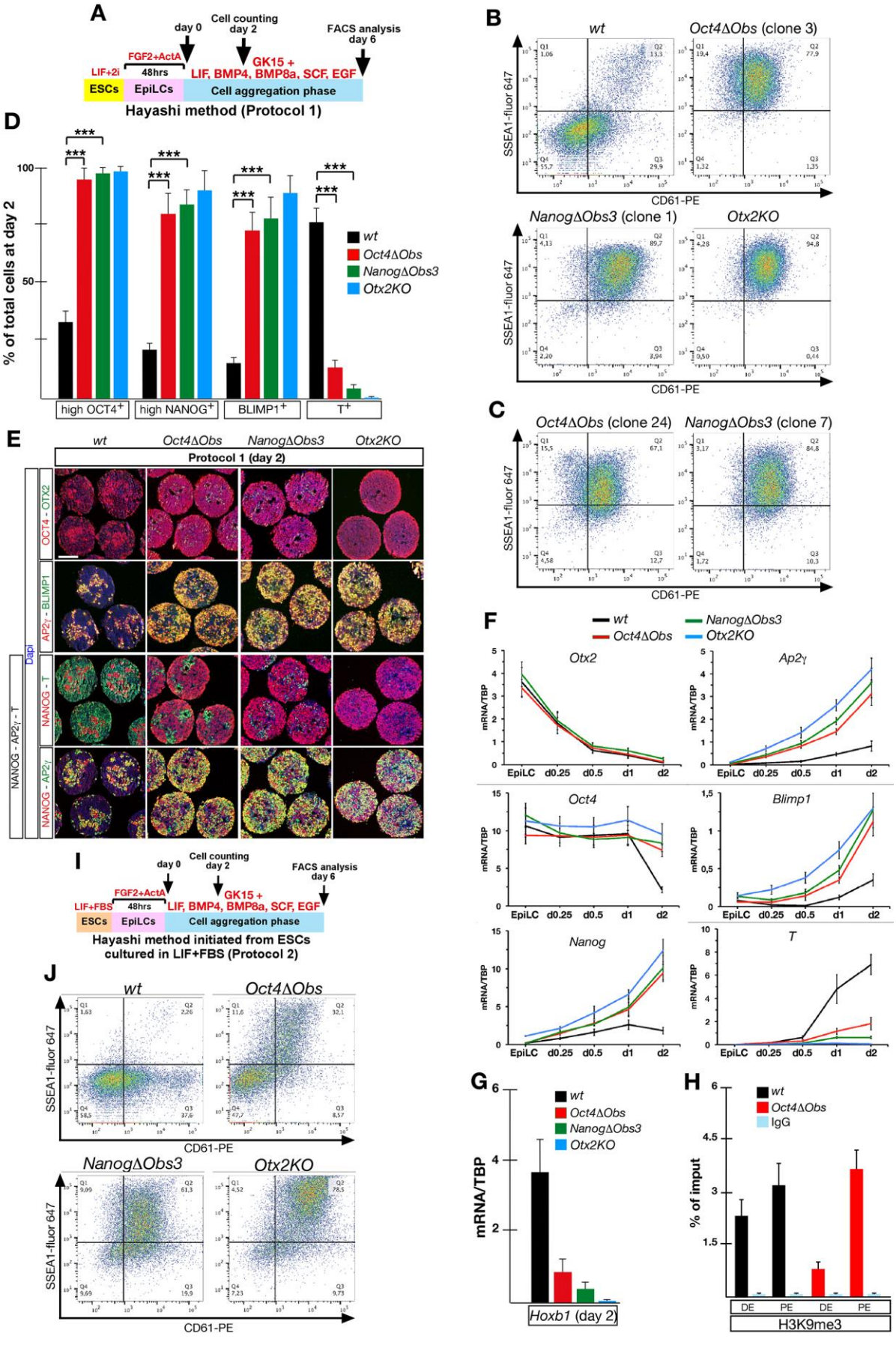

**Fig. 2. OTX2 binding to *Oct4* or *Nanog* enhancer region regulates PGCLC and somatic mesoderm differentiation.** (A) Protocol 1 experimental design. (B,C) FACS analysis performed at d6 on wt, Δ*Obs* and *Otx2KO* cell aggregates with SSEA1 and CD61 antibodies. (D) Counting at d2 of cells expressing the indicated TFs in wt and mutants. Data are the mean ± SD of 3 independent experiments. *P* value: *= between 0,005 and 0,001; **=<0,001; and ***=<<0,001. (E) Representative immunostainings performed at d2 on sections from wt, Δ*Obs* and *Otx2KO* cell aggregates using the indicated antibodies. Sections were counterstained with Dapi. Scale bar = 100µm. (F,G) RT-qPCR analysis showing the expression profile of *Otx2*, *Oct4*, *Nanog*, *Ap2γ*, *Blimp1* and *T* in EpiLCs and in cell aggregates at d0.25, d0.5, d1 and d2 (F) and *Hoxb1* expression at d2 (G). Data were normalized to *TBP* mRNA and reported as the mean ± SD of 3 independent experiments. (H) ChIP-qPCR analysis performed at d2 in wt and *Oct4*Δ*Obs* cell aggregates to assess the H3K9me3 enrichment level on the DE and PE of *Oct4*. Data are the mean ± SD of 3 independent experiments. (I) Protocol 2 experimental design. (J) FACS analysis at d6 on wt, Δ*Obs* and *Otx2KO* cell aggregates with SSEA1 and CD61 antibodies.

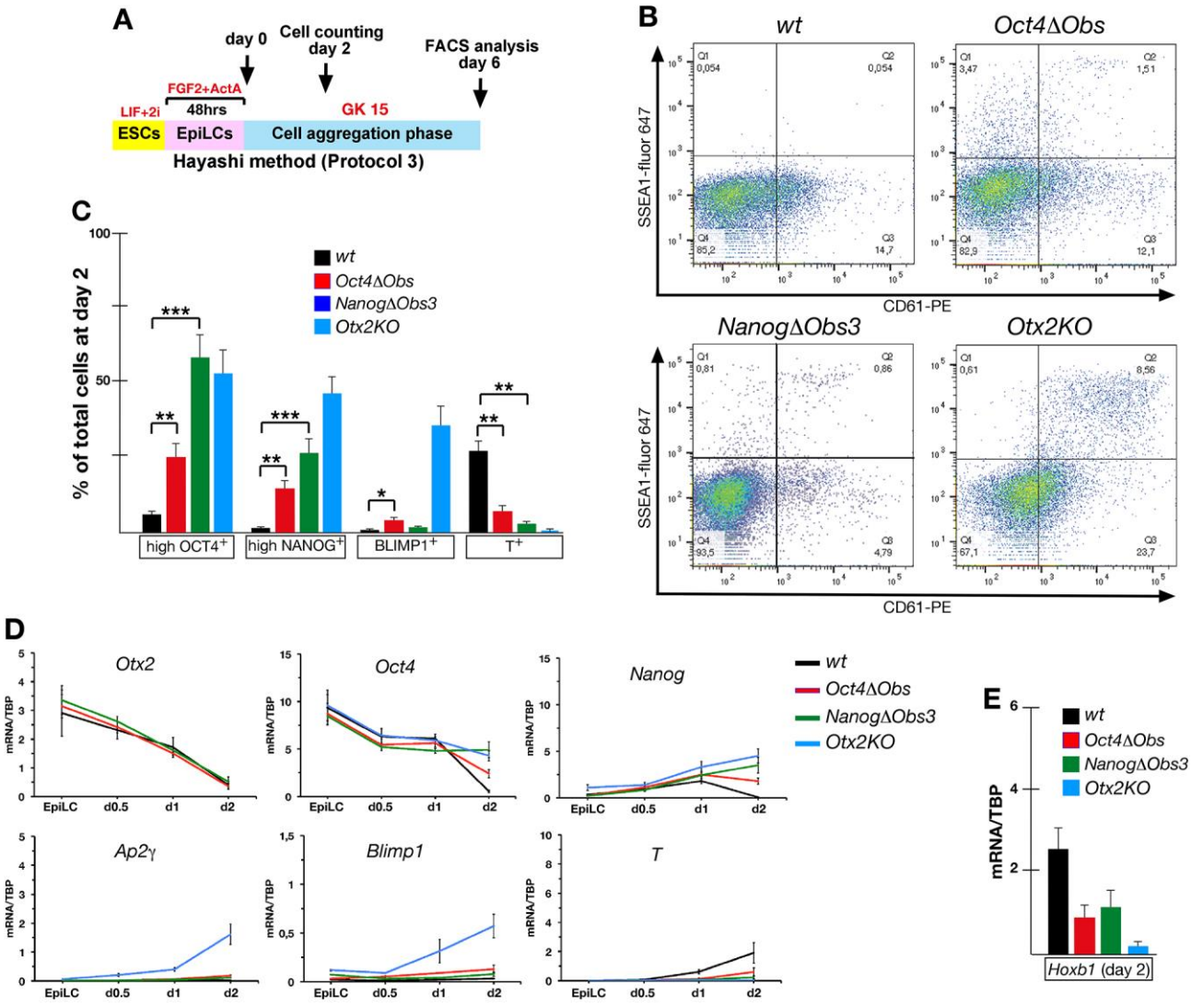


**Fig. 3. Cytokines requirement for PGCLC differentiation in Δ*Obs* mutants.** (A) Protocol 3 experimental design. (B) FACS analysis for SSEA1 and CD61 at d6 on wt, Δ*Obs* and *Otx2KO* cell aggregates. (C) Counting at d2 of cells expressing the indicated TFs in wt and mutants. Data are the mean ± SD of 3 independent experiments. *P* value: *=between 0,005 and 0,001; **=<0,001; ***=<<0,001. (D,E) RT-qPCR analysis of the indicated transcripts at the time points shown (D), and *Hoxb1* expression at d2 (E). Data were normalized to *TBP* mRNA and reported as the mean ± SD of 3 independent experiments.

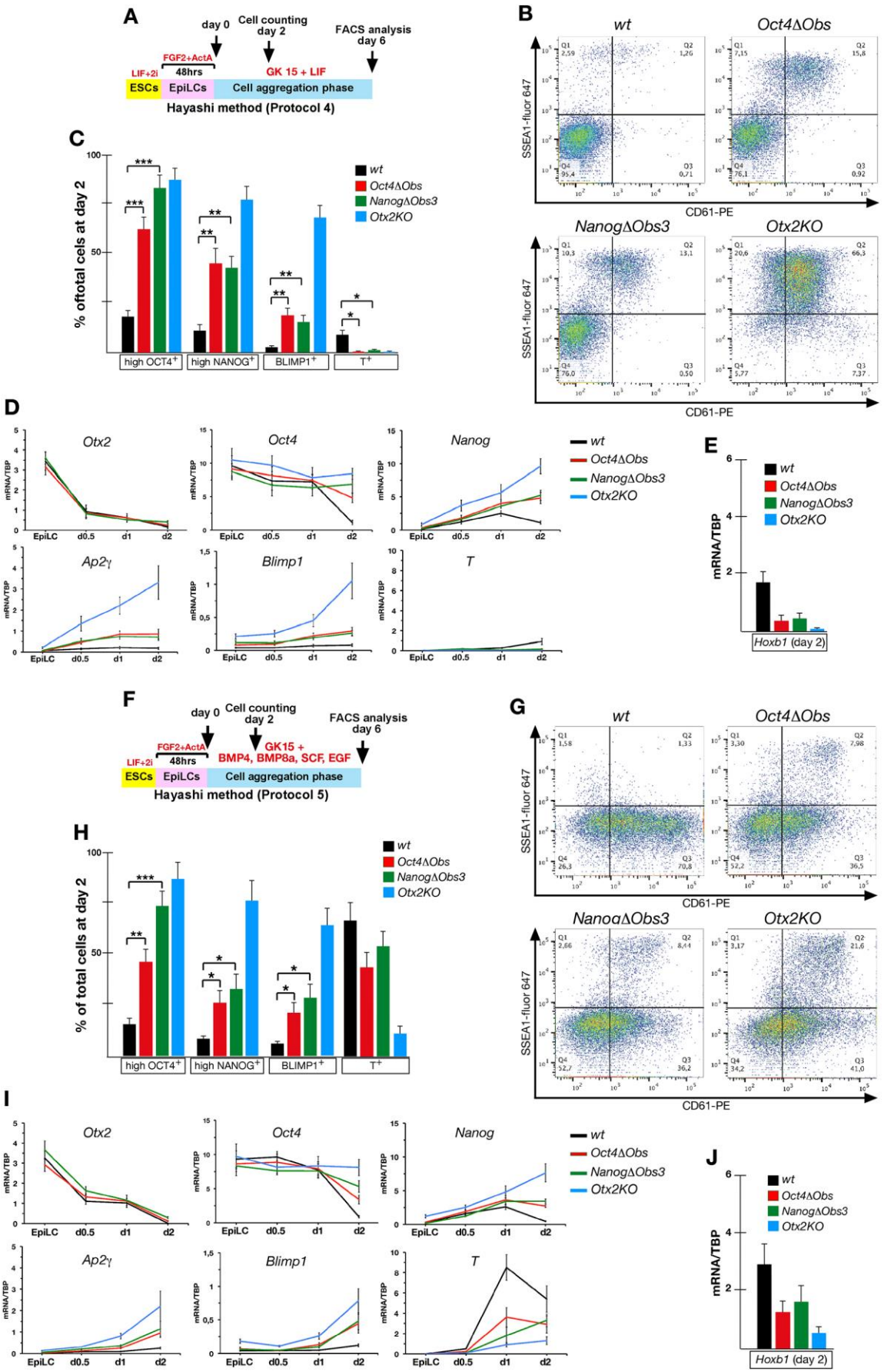

**Fig. 4. In Δ*Obs* mutants LIF stimulates PGCLC differentiation and suppresses somatic fate more efficiently than BMP4**. (A) Protocol 4 experimental design. (B) FACS analysis for SSEA1 and CD61 at d6 on wt, Δ*Obs* and *Otx2KO* cell aggregates. (C) Counting at d2 of cells expressing the indicated TFs in wt and mutants. (D,E) RT-qPCR analysis of the indicated transcripts at the time points shown (D) and *Hoxb1* expression at d2 (E). (F) Protocol 5 experimental design. (G) FACS analysis for SSEA1 and CD61 at d6 on wt, Δ*Obs* and *Otx2KO* cell aggregates. (H) Counting at d2 of cells expressing the indicated TFs in wt and mutants. (I,J) RT-qPCR analysis of the indicated transcripts at the time points shown (I), and *Hoxb1* expression at d2 (J). (C,H) Data are the mean ± SD of 3 independent experiments. *P* value: *=between 0,005 and 0,001; **=<0,001 and ***=<<0,001. (D,E,I,J) Data were normalized to *TBP* mRNA and reported as the mean ± SD of 3 independent experiments.

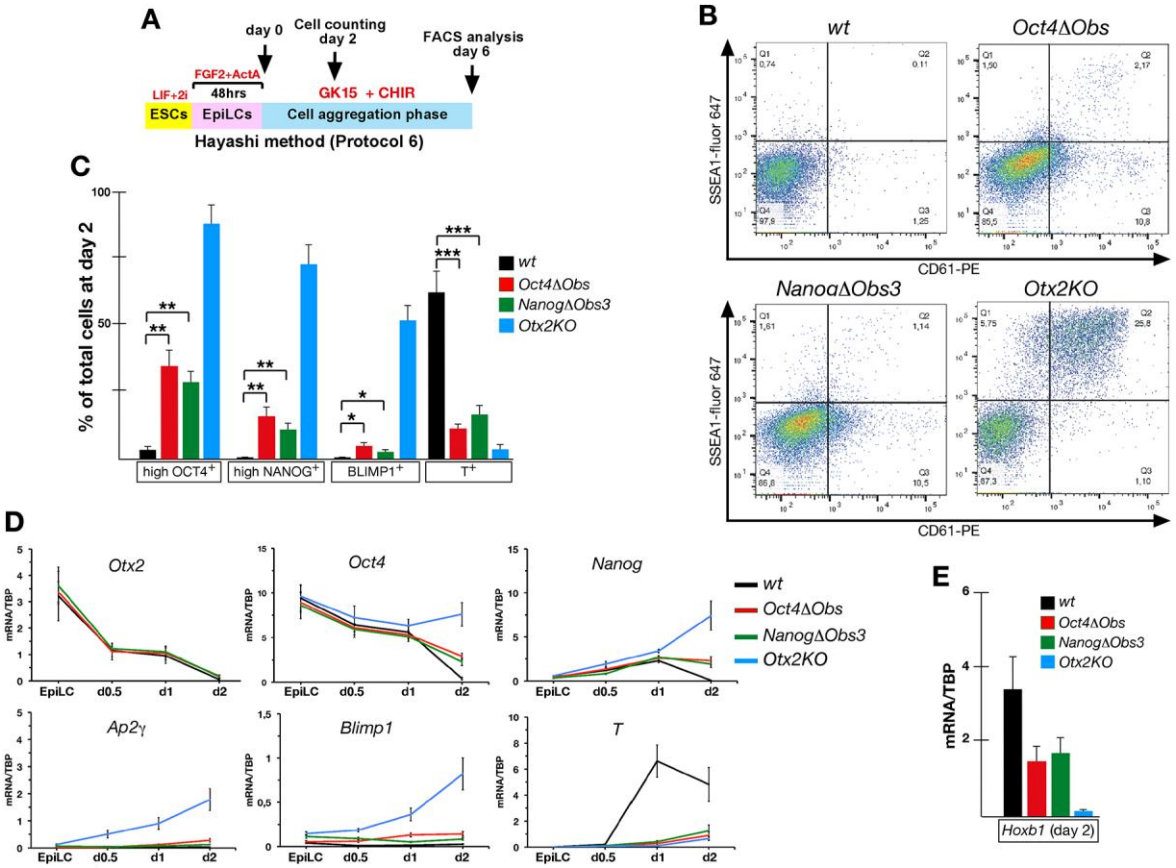


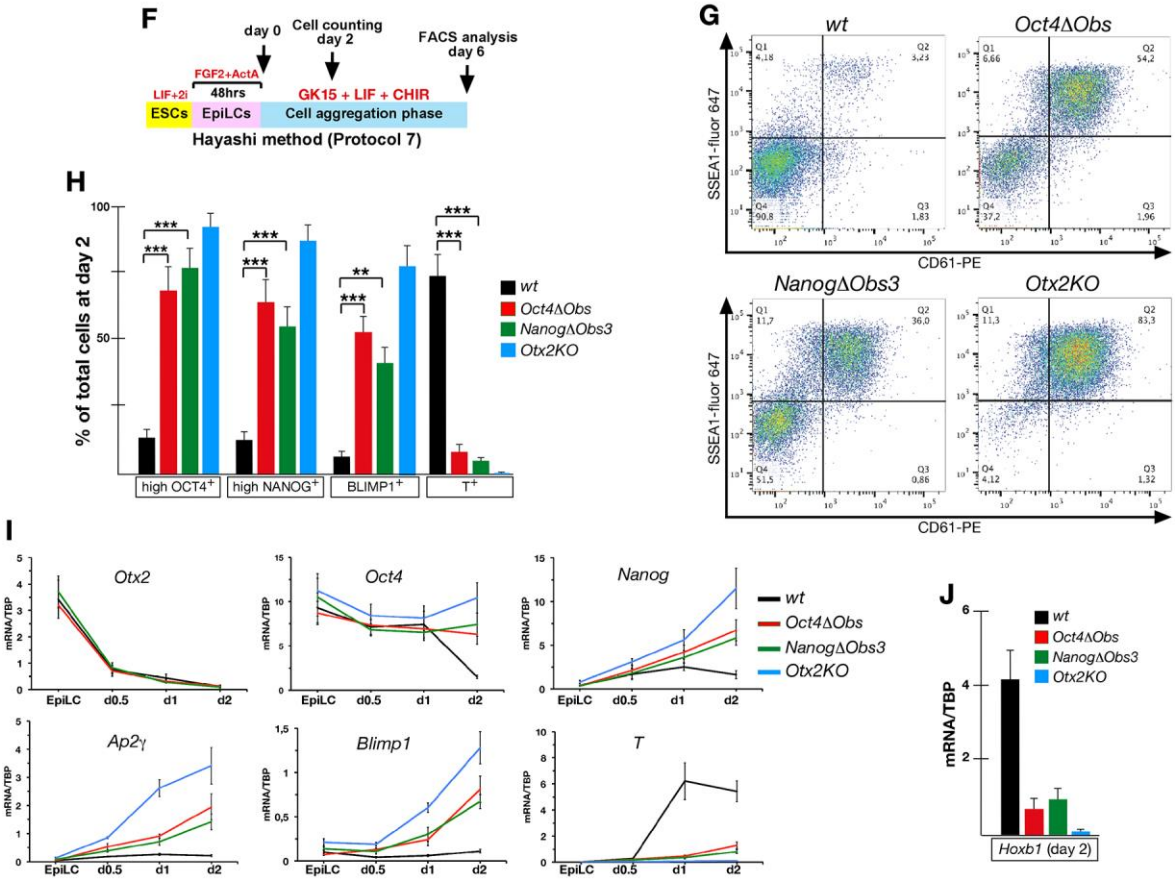

**Fig. 5. Germline entry of Δ*Obs* mutants is enhanced by LIF in conjunction with CHIR.** (A) Protocol 6 experimental design. (B) FACS analysis for SSEA1 and CD61 at d6 on wt, Δ*Obs* and *Otx2KO* cell aggregates. (C) Counting at d2 of cells expressing the indicated TFs in wt and mutants. (D,E) RT-qPCR analysis of the indicated transcripts at the time points shown (D), and *Hoxb1* expression at d2 (E). (F) Protocol 7 experimental design. (G) FACS analysis for SSEA1 and CD61 at d6 on wt, Δ*Obs* and *Otx2KO* cell aggregates. (H) Counting at d2 of cells expressing the indicated TFs in wt and mutants. (I,J**)** RT-qPCR analysis of the indicated transcripts at the time points shown (I), and *Hoxb1* expression at d2 (J). (C,H) Data are the mean ± SD of 3 independent experiments. *P* value: *=between 0,005 and 0,001; **=<0,001 and ***=<<0,001. (D,E,I,J) Data were normalized to *TBP* mRNA and reported as the mean ± SD of 3 independent experiments.

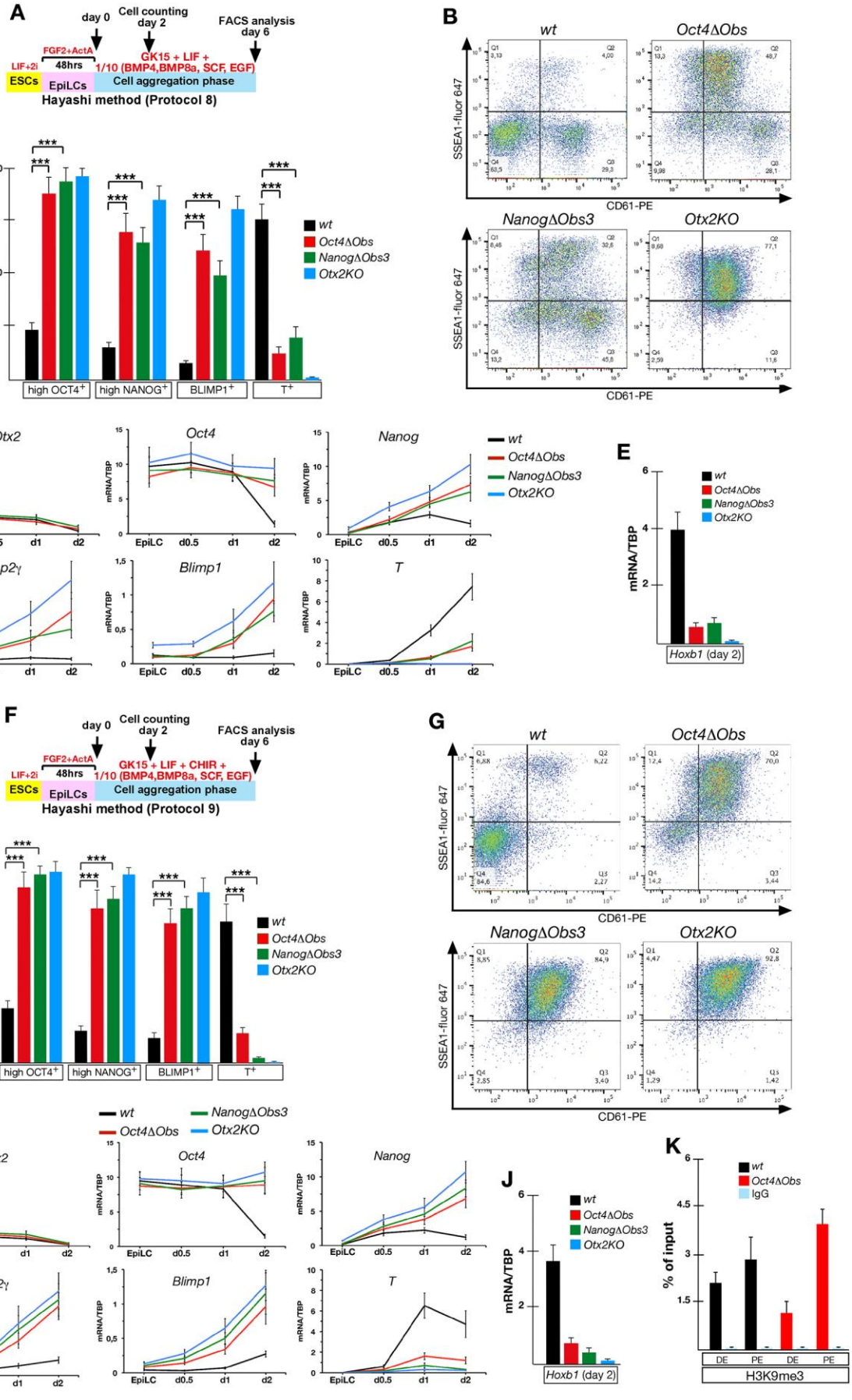

**Fig. 6. Germline entry of Δ*Obs* mutants is markedly increased by LIF in synergism with CHIR and low dosage of BMP4, BMP8a, SCF and EGF.** (A) Protocol 8 experimental design. (B) FACS analysis for SSEA1 and CD61 at d6 on wt, Δ*Obs* and *Otx2KO* cell aggregates. (C) Counting at d2 of cells expressing the indicated TFs in wt and mutants. (D,E) RT-qPCR analysis of the indicated transcripts at the time points shown (D), and *Hoxb1* expression at d2 (E). (F) Protocol 9 experimental design. (G) FACS analysis for SSEA1 and CD61 at d6 on wt, Δ*Obs* and *Otx2KO* cell aggregates. (H) Counting at d2 of cells expressing the indicated TFs in wt and mutants. (I,J) RT-qPCR analysis of the indicated transcripts at the time points shown (I), and *Hoxb1* expression at d2 (J). (K) ChIP-qPCR analysis performed at d2 in wt and *Oct4*Δ*Obs* cell aggregates to assess the H3K9me3 enrichment level on the DE and PE of *Oct4*. Data are the mean ± SD of 3 independent experiments. (C,H) Data are the mean ± SD of 3 independent experiments. *P* value: *=between 0,005 and 0,001; **=<0,001 and ***=<<0,001. (D,E,I,J) Data were normalized to *TBP* mRNA and reported as the mean ± SD of 3 independent experiments.

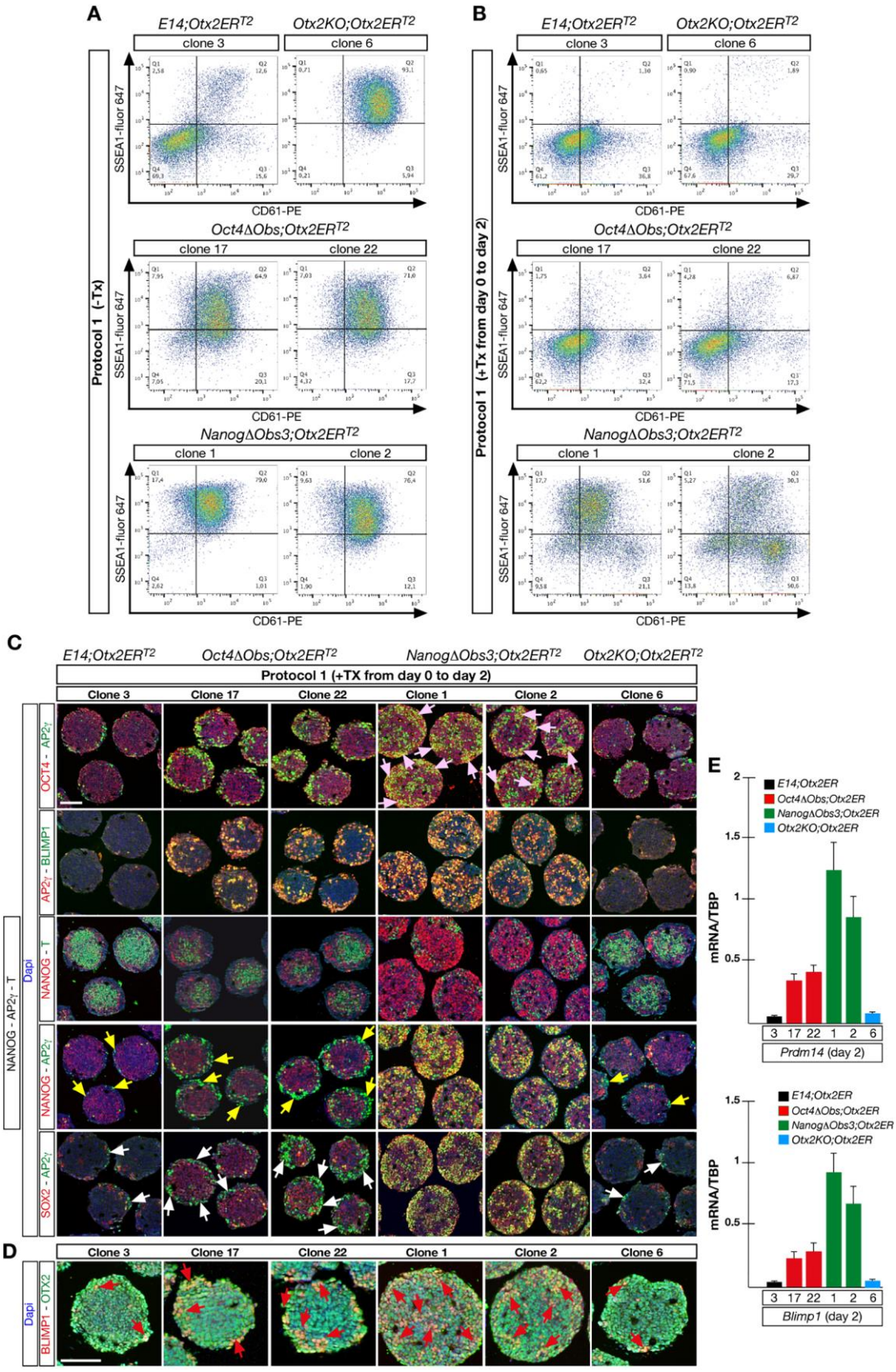

**Fig. 7. Nuclear translocation of *OTX2-ER$^{T2}$* attenuates without suppressing germline entry of *Oct4ΔObs* and *NanogΔObs3* cell lines.** (A,B) FACS analysis for SSEA1 and CD61 at d6 on the indicated mutant cell lines cultured according to protocol 1 with (A) or without (B) Tx from d0 to d2. (C) Immunohistochemistry experiments performed at d2 on representative sections from Tx-treated cell lines stained with the indicated antibodies. Note that AP2$\gamma^{+}$ PGCLCs co-express high NANOG (yellow arrows), SOX2 (white arrows) and high OCT4 (pink arrows) only in *NanogΔObs3;Otx2ER$^{T2}$* cells. (D) Immunostaining assays showing that OTX2-ER$^{T2}$ is co-expressed with BLIMP1 in all cell lines (red arrows). Sections were counterstained with Dapi. Scale bar = 100µm. For *Oct4ΔObs;Otx2ER$^{T2}$* and *NanogΔObs3;Otx2ER$^{T2}$* mutants, two independent clones were analyzed. (E) RT-qPCR analysis performed at d2 to determine the expression level of *Prdm14* and *Blimp1* in all cell lines. Data were normalized to *TBP* mRNA and reported as the mean ± SD of 3 independent experiments.

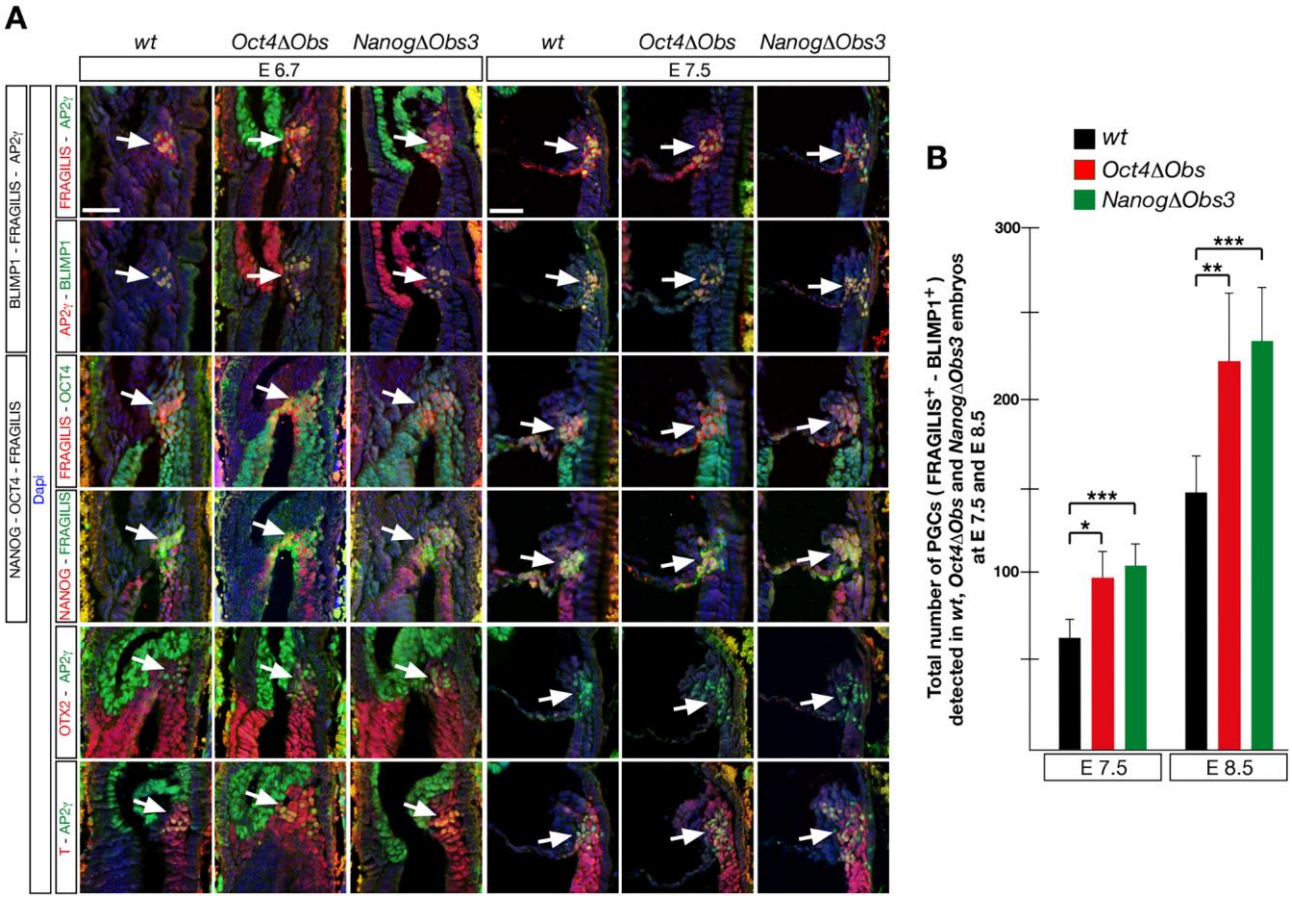


**Fig. 8. Increased generation of PGCs in Δ*Obs* mutant embryos.** (A) Immunohistochemistry analysis of wt and Δ*Obs* homozygous embryos at E6.7 and E7.5 using the indicated antibodies. Sections were counterstained with Dapi. Arrow points to PGCs. Scale bar = 50μm. (B) PGC counting data collected in wt and Δ*Obs* embryos at E7.5 and E8.5. The number of PGCs is reported as mean ± SD. *P* value: *= between 0,005 and 0,001; **=<0,001 and ***=<<0,001.

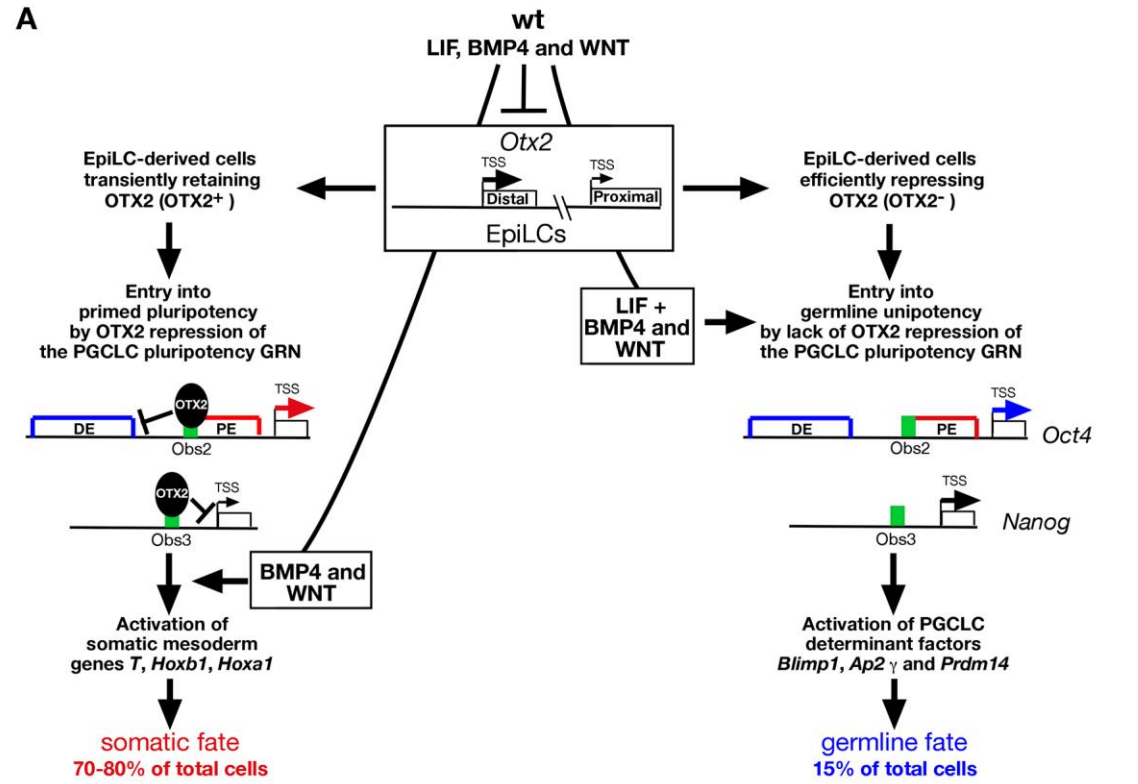


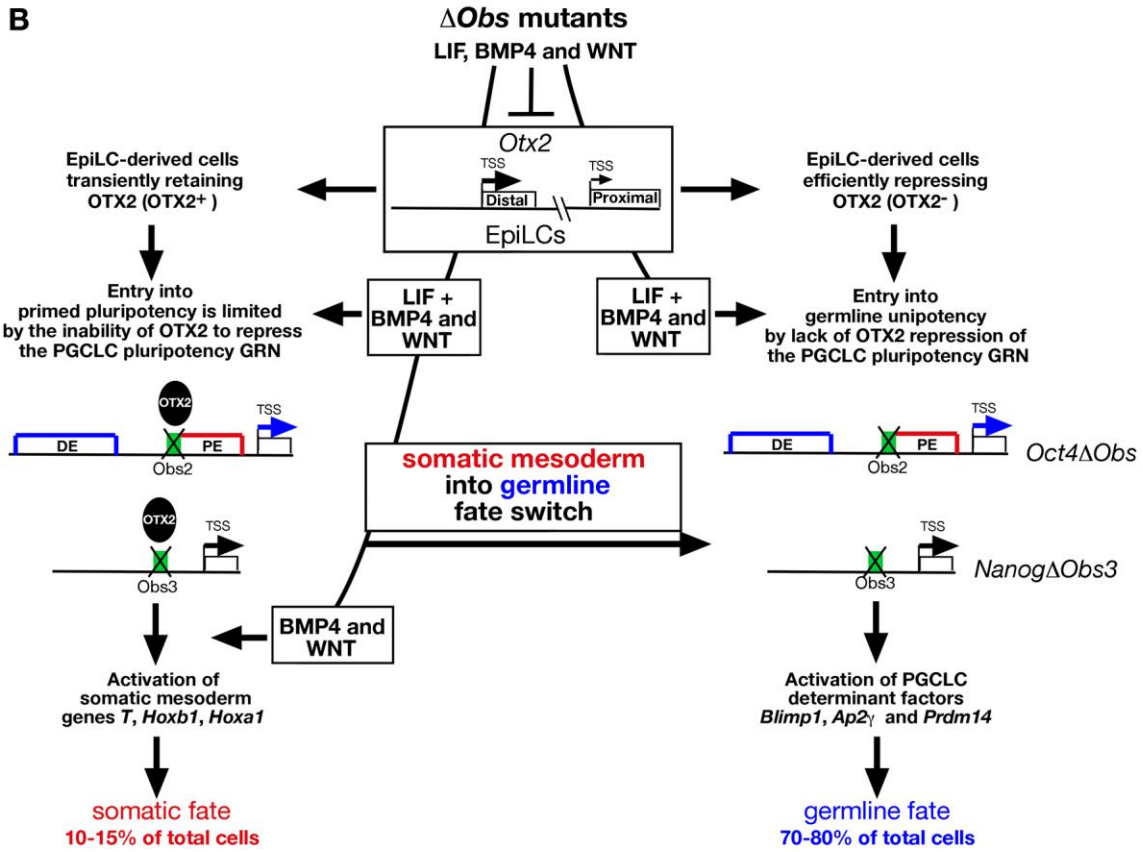

**Fig. 9. Model of OTX2 action in germline and somatic mesoderm differentiation.** Diagram illustrating the role of OTX2 in controlling the contribution of EpiLC-derived cells to germline and somatic mesoderm. (A) During the cell aggregation phase, *Otx2* suppression by LIF, BMP4 and WNT generates $OTX2^+$ and $OTX2^-$ cell subtypes. $OTX2^-$ cells (on the right) activate the PGCLC pluripotency GRN and supported by cytokine-dependent stimulation of proliferation enter the germline differentiation program to generate PGCLCs in 15% of the population; $OTX2^+$ cells (on the left) enter primed pluripotency via OTX2 repression of the PGCLC pluripotency GRN and generate somatic mesoderm cells in about 70-80% of the population. (B) In Δ*Obs* mutants, the initial steps giving rise to the $OTX2^-$ and $OTX2^+$ cell subtypes and the germline fate of the $OTX2^-$ cell subtype (on the right) are apparently unaffected. In contrast, entry into primed pluripotency of the $OTX2^+$ cell subtype (on the left) is limited by the inability of OTX2 to repress the pluripotency GRN, which together with cytokines promote germline differentiation. This is reflected by a switch from somatic into germline fate in both Δ*Obs* mutants. The distal and proximal transcription start sites (TSSs) of *Otx2* are indicated. The DE and PE of *Oct4* are framed in blue and red, with the blue and red horizontal arrows corresponding to *Oct4* transcripts driven by the DE and PE, respectively. The size of the horizontal arrow in correspondence of the TSS of *Nanog* and in correspondence of the TSSs of *Otx2* is proportional to the transcriptional activity. The green boxes correspond to Obs2 for *Oct4* and to Obs3 for *Nanog*.

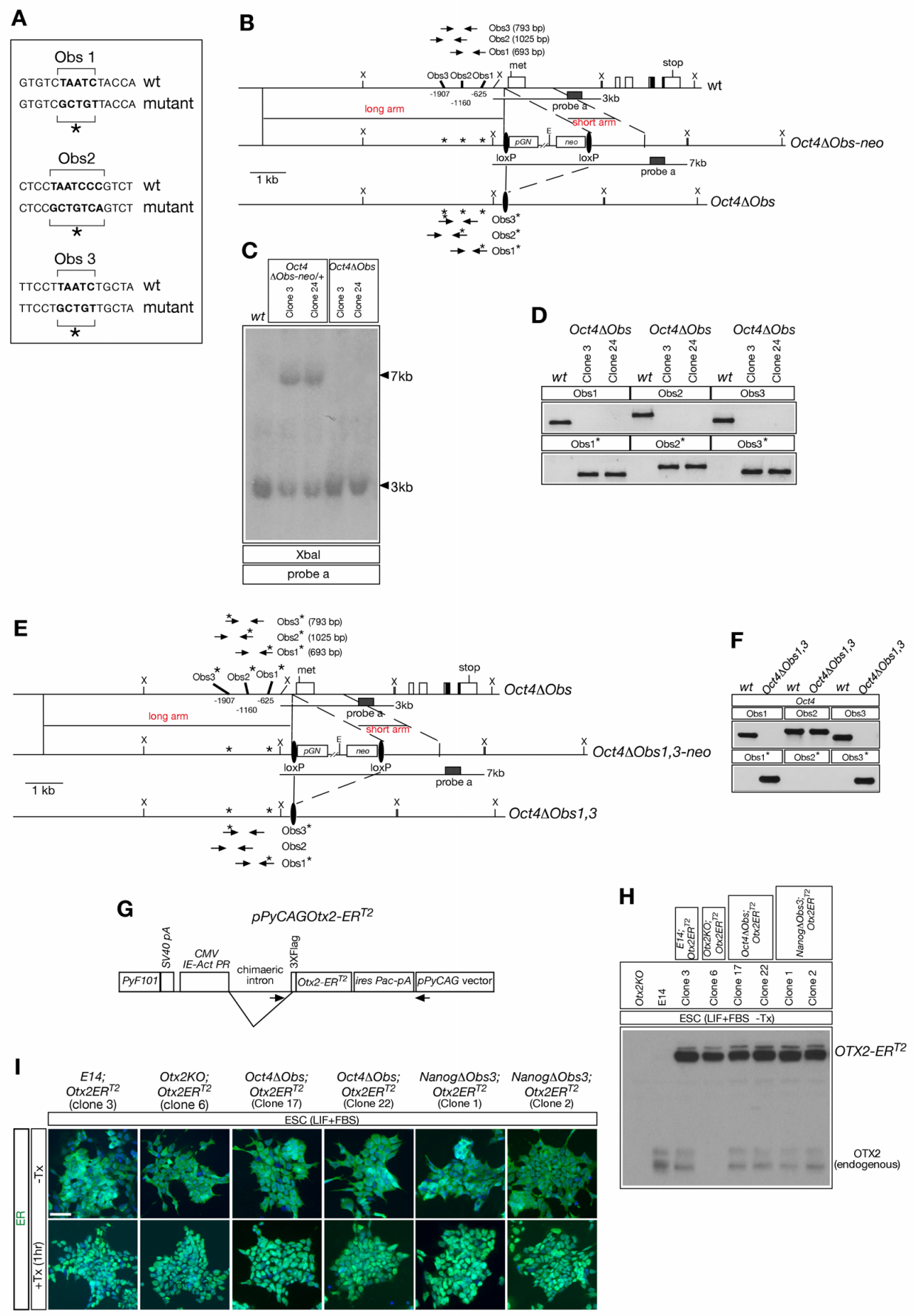


**Figure S1. Generation of mutant ESC lines.** (A) Obs1, 2 and 3 wt and mutagenized sequences (*) located within the *Oct4* enhancer region. (B) Targeting strategy adopted to generate the *Oct4ΔObs* allele through the intermediate generation of the *Oct4ΔObs-neo* allele. The upper line shows the *Oct4* locus

with exon-intron organization and the region upstream of the methionine (met) where Obs1, Obs2 and Obs3 are located; the *Oct4* stop codon is indicated; primers specific for the Obs wt sequences and length of the amplified region are also shown. Second line shows the *Oct4*Δ*Obs-neo* allele which carries the Obs mutagenized sequence (*) and the *loxP-pGN-neo-loxP* cassette; removal of this cassette through transient expression of a *Cre* recombinase expressing vector generated the *Oct4*Δ*Obs* allele (third line). *Oct4*Δ*Obs*/+ cells were used to target the second *Oct4* allele. The *loxP* cassette was removed from the second targeting event to produce *Oct4*Δ*Obs* homozygous cells used for Southern and PCR analyses. Primers specific for genotyping of Obs mutated sequences are shown below the third line. Filled ovals indicate the *loxP* sites; probe a corresponds to the filled rectangular box; X stands for the XbaI restriction enzyme. (C) Southern blot of wt, *Oct4*Δ*Obs-neo*/+ and *Oct4*Δ*Obs* homozygous ESC clones with probe a showing wt and mutant alleles; *Oct4*Δ*Obs* homozygous clones showed a band differing from wt only for the length of the *loxP* sequence. (D) PCR assays on wt and *Oct4*Δ*Obs* ESCs with oligonucleotides recognizing the wt or the mutagenized Obs1, 2 and 3 sequences. (E) Targeting strategy to generate the *Oct4*Δ*Obs1,3* ESC line showing the *Oct4*Δ*Obs* locus (upper line), the *Oct4*Δ*Obs1,3-neo* intermediate allele (second line), and the *Oct4*Δ*Obs1,3* locus (third line). The latter was generated by CRE recombinase-mediated removal of the *pGN-neo* cassette. *Oct4*Δ*Obs1,3*/+ cells were used to target the second *Oct4* allele. The *loxP* cassette was removed from the second targeting event to produce *Oct4*Δ*Obs1,3* homozygous cells. Mutant (*) and wt Obs oligonucleotides are indicated; filled ovals correspond to *loxP* sequence and probe a used in Southern blot assays corresponds to the filled rectangle. (F) PCR assays performed on wt and homozygous *Oct4*Δ*Obs1,3* ESCs showed that in *Oct4*Δ*Obs1,3* the mutated Obs2 sequence has been reverted to the wt version. (G) Schematic representation of *pPyCAGOtx2-ER$^{T2}$* plasmid. (H) Western blot hybridized with the OTX2 antibody showing the expression of the endogenous OTX2 compared to that of the *OTX2-ER$^{T2}$* transgene in *E14;Otx2ER$^{T2}$*, *Otx2KO;Otx2ER$^{T2}$*, *Oct4*Δ*Obs;Otx2ER$^{T2}$* and *Nanog*Δ*Obs3;Otx2ER$^{T2}$* selected clones. *E14* and *Otx2KO* ESCs were included as control extracts.

(I) Immunostaining assays performed on selected clones with the ER antibody to detect the distribution of the OTX2-ER$^{T2}$ fusion protein in the absence or after 1 hour of exposure to Tx; an efficient nuclear translocation of OTX2-ER$^{T2}$ was induced by Tx.

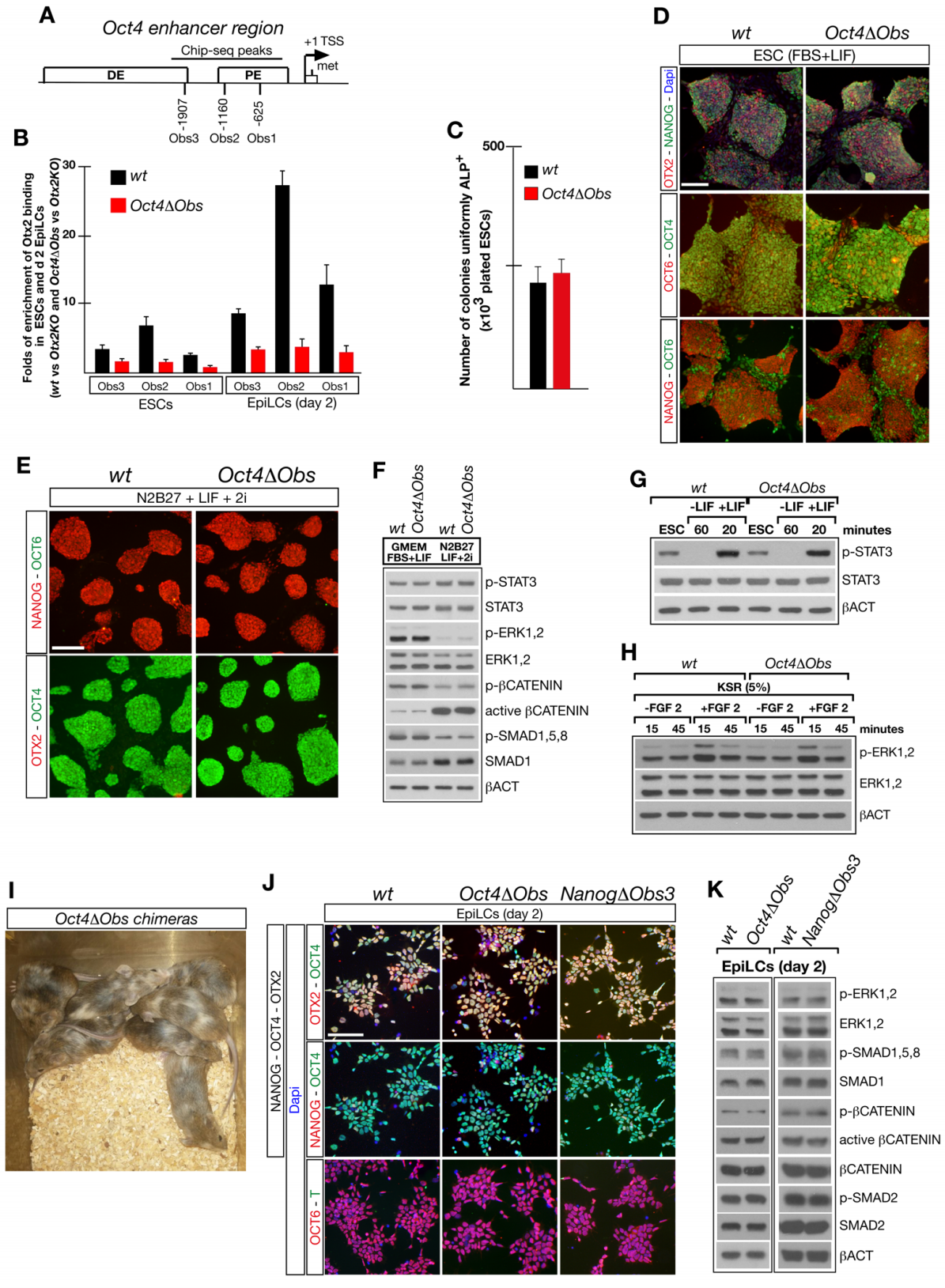


**Figure S2. Analysis of *Oct4ΔObs* ESCs and Δ*Obs* EpiLCs.** (A) Schematic representation of the *Oct4* genomic region located upstream of the transcription start site (TSS) showing the position of Obs1-3 in relation to the proximal (PE) and distal (DE) enhancers; the distance of the Obs from the TSS is indicated. (B) ChIP assays showing that compared to wt, the OTX2 binding to Obs1-3 was virtually abrogated in *Oct4ΔObs* ESC and EpiLCs. Data were collected from 3 independent experiments and

reported as mean ± SD. (C) Graphic representation showing that the number of $ALP^+$ uniformly stained ESC colonies was comparable in wt and *Oct4*Δ*Obs* ESCs. Data were collected from 3 independent experiments and reported as mean ± SD. (D) Representative immunostaining assays with OTX2 and NANOG, with OCT6 and OCT4, and with NANOG and OCT6 revealed a very similar distribution of these markers in wt and *Oct4*Δ*Obs* ESCs cultured in FBS+LIF. Dapi was employed to counterstain only ESCs immunostained with OTX2 and NANOG; scale bar = 100µm. (E) Conversion to the naïve state by sequential passages in N2B27 medium plus LIF and 2i showed no difference between wt and *Oct4*Δ*Obs* ESCs in the expression of NANOG, OCT6, OTX2 and OCT4; indeed, while OTX2 and OCT6 were suppressed, OCT4 and NANOG were uniformly expressed at high level. Scale bar = 100µm. (F) Western blot analysis on ESCs cultured in FBS+LIF or LIF+2i showed that the expression of p-STAT3, STAT3, p-ERK1,2, ERK1,2, p-βCATENIN, active βCATENIN, p-SMAD1,5,8, SMAD1 was very similar in wt and *Oct4*Δ*Obs* ESCs. β-ACTIN was used to normalize protein extracts. (G,H) *wt* and *Oct4*Δ*Obs* ESCs showed similar response to LIF (G) or FGF2 (H) addition as revealed by Western blot analysis with p-STAT3 and STAT3 (G) or p-ERK1,2 and ERK1,2 (H). β-ACTIN was used to normalize protein extracts. (I) *Oct4*Δ*Obs* ESCs showed efficient chimerism when injected into host blastocysts. (J,K) Immunostaining (J) and Western blot (K) assays showed that wt and Δ*Obs* EpiLCs exhibited at d2 a very similar distribution of OTX2, OCT4, NANOG and OCT6, did not express T (J) and showed a similar expression level also for p-ERK1,2, ERK1,2, p-SMAD1,5,8, SMAD1, p-βCATENIN, active βCATENIN; βCATENIN, p-SMAD2 and SMAD2 (K). Scale bar in J = 100µm.

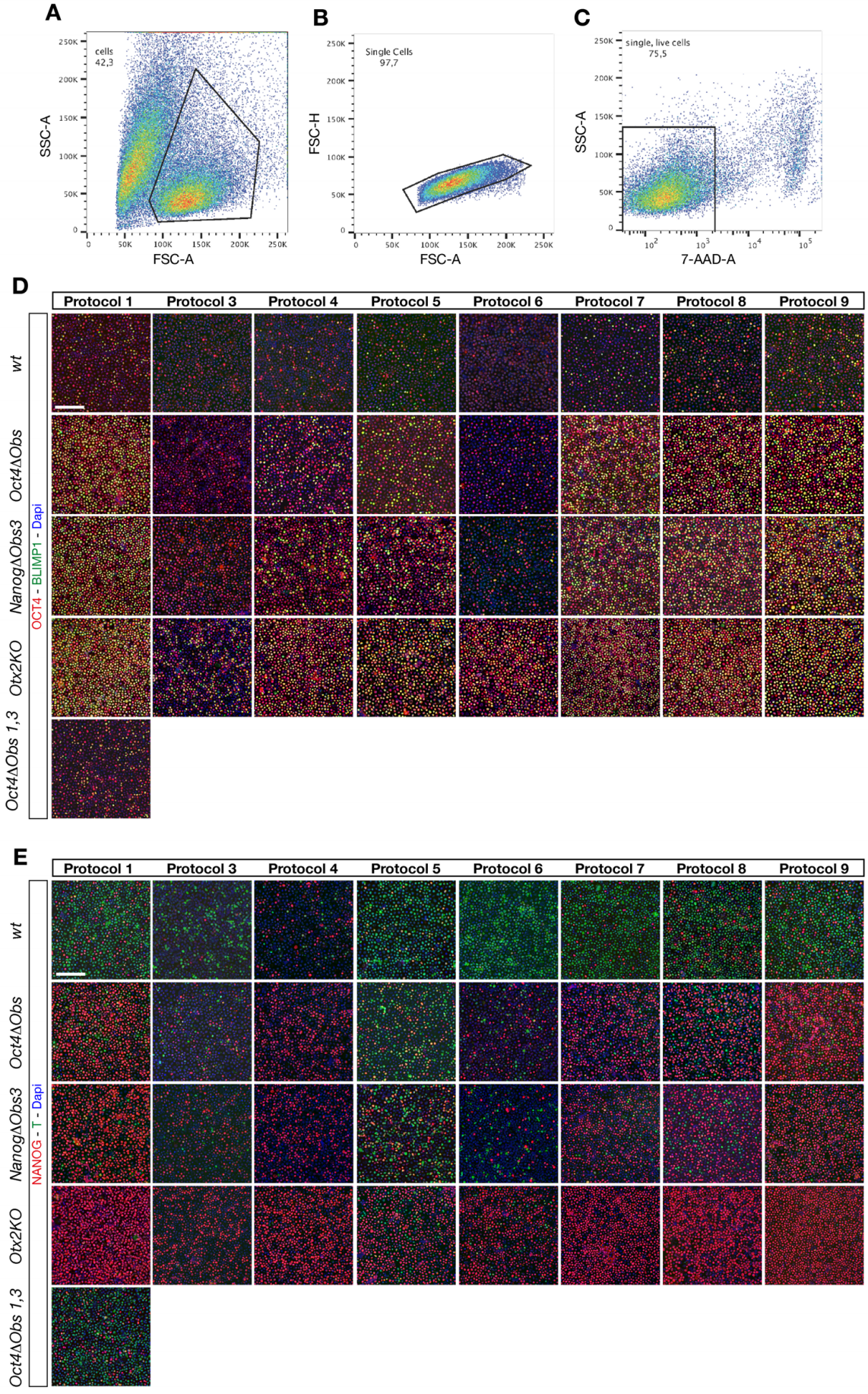


**Figure S3. FACS gating strategy and cytospin assays for cell counting in d2 cell aggregates.** (A-C) *NanogΔObs3* d6 cell aggregates were used as a representative example to show the gating strategy

in which dissociated cells were first gated on the basis of the FSC (size) and SSC (complexity) scatter plot. (B) Single cells were then selected based on the linear correlation between the FSC-area (FSC-A) and the FSC-height (FSC-H). (C) Dead cells were excluded by 7-AAD dye. (D,E) Representative immunostaining assays with OCT4 and BLIMP1 (D) and NANOG and T (E) on cytospun cells from dissociated wt, Δ*Obs*, *Oxt2KO* and *Oct4*Δ*Obs1,3* EpiLC-derived cell aggregates cultured up to d2 according to protocols 1, 3-9. Cells were counterstained with Dapi; 3 independent experiments for each cell line and for each protocol were performed to collect cell counting data.

Scale bars = 100μm.

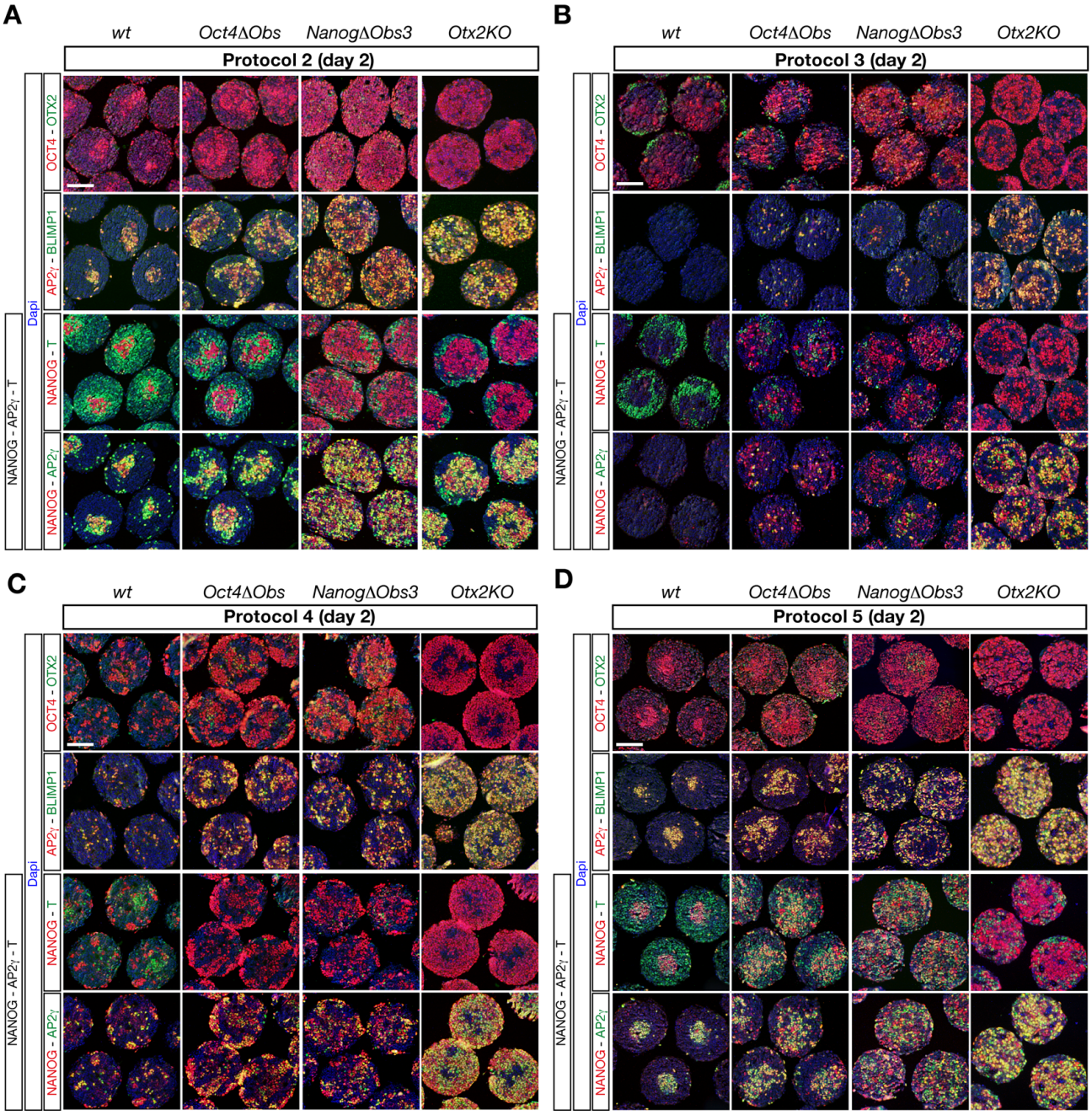


**Figure S4. Expression analysis in d2 cell aggregates.** (A-D) Representative immunohistochemistry experiments on wt, Δ*Obs* and *Otx2KO* sections of d2 cell aggregates generated according to protocols 2 (A), 3 (B), 4 (C) and 5 (D). Sections were immunostained with OTX2 and OCT4, with AP2γ and BLIMP1 and with NANOG, T and AP2γ antibodies. Sections were counterstained with Dapi. Immunostainings were performed on at least two independent experiments for each protocol. Scale bars = 100µm.

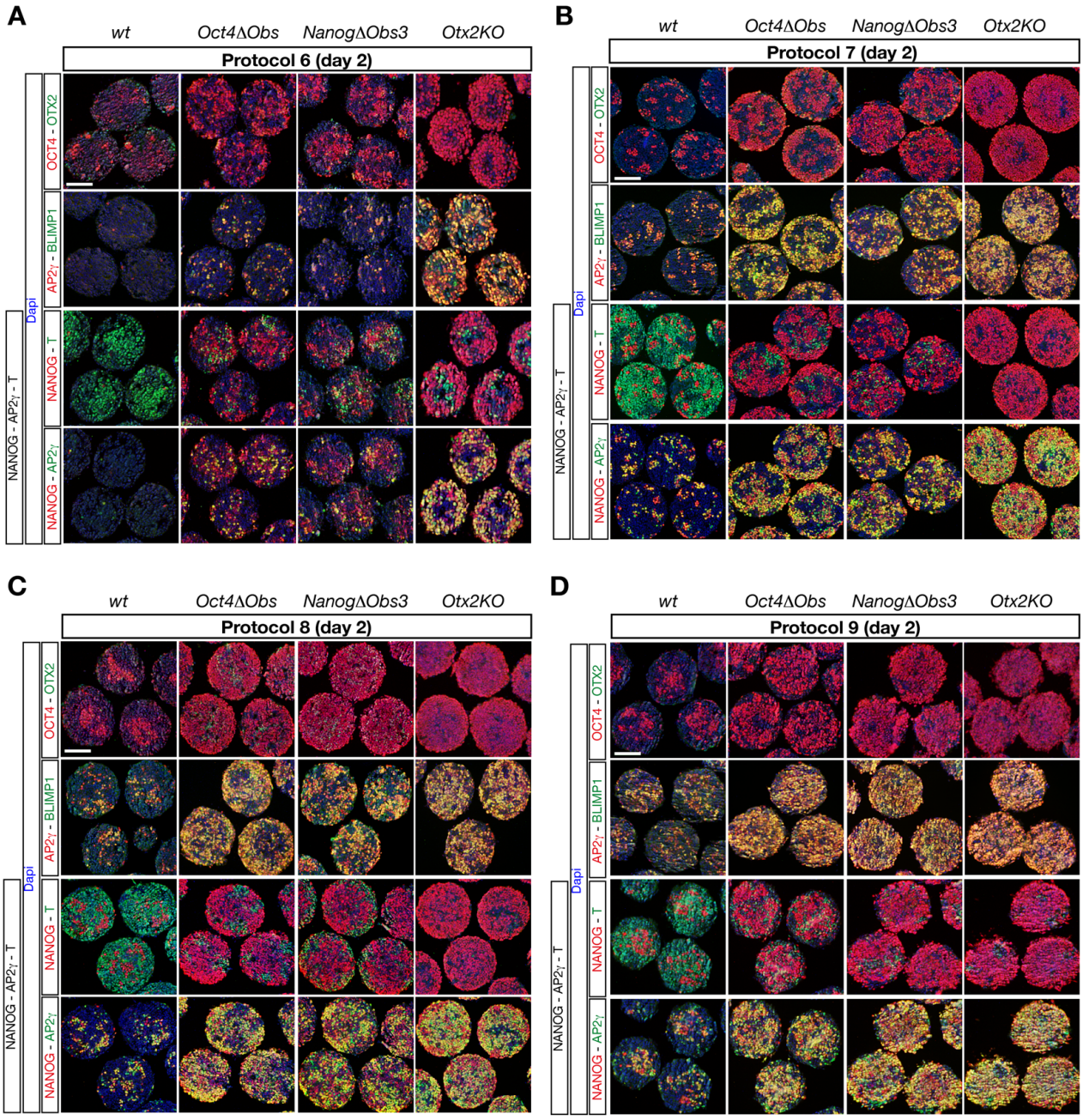


**Figure S5. Expression analysis in d2 cell aggregates.** (A-D) Representative immunohistochemistry experiments performed at d2 on wt, Δ*Obs* and *Otx2KO* cell aggregates generated according to protocols 6 (A), 7 (B), 8 (C) and 9 (D). Sections were immunostained with OTX2 and OCT4, with AP2γ and BLIMP1, and with NANOG, T and AP2γ antibodies. Sections were counterstained with Dapi. Immunostainings were performed on at least two independent experiments for each protocol. Scale bars = 100µm.

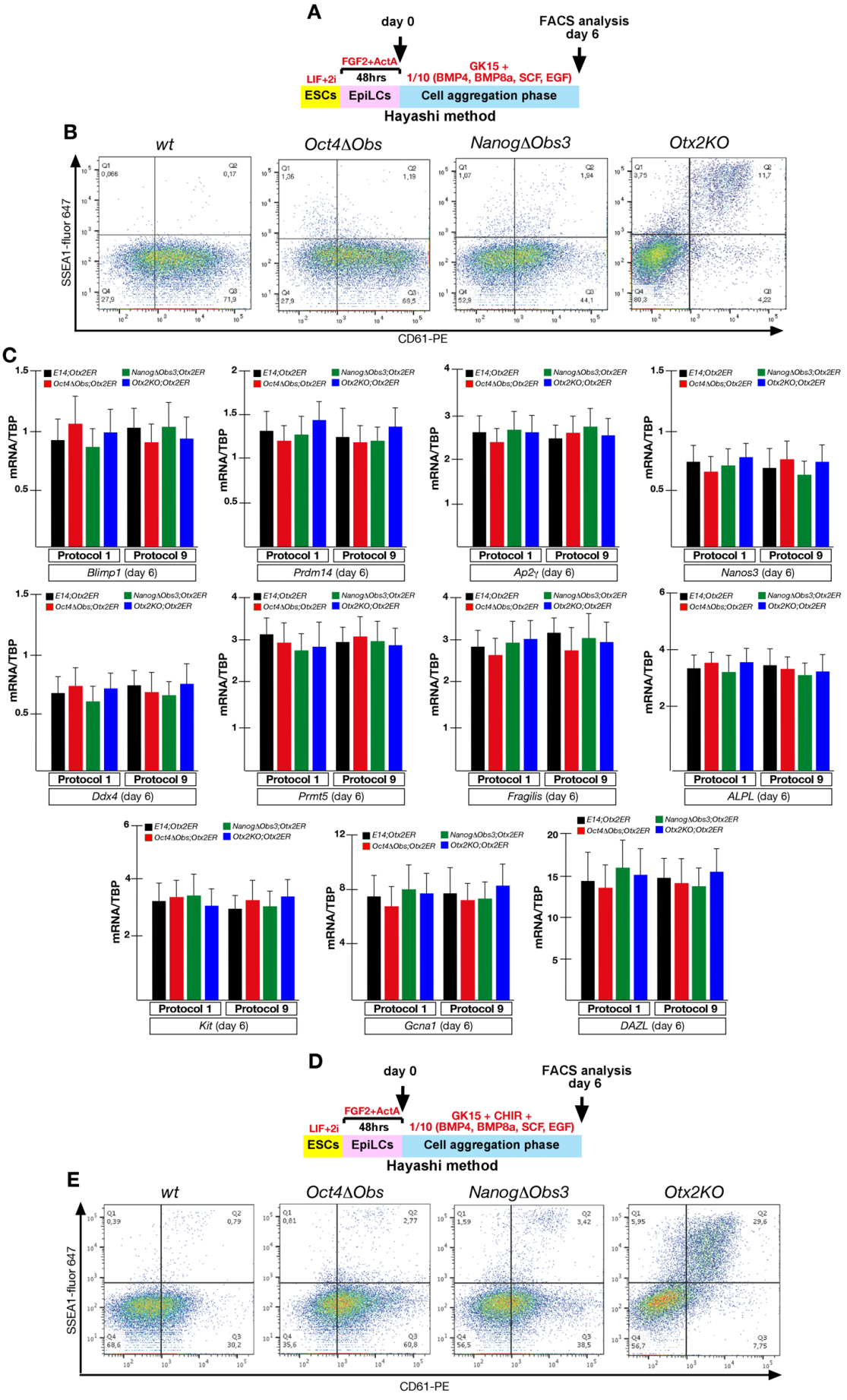


**Figure S6. Effects of low dosage of BMP4, BMP8a, EGF and SCF alone or in combination with CHIR on PGCLC induction and expression analysis in PGCLCs purified from d6 cell**

**aggregates cultured according to protocols 1 and 9.** (A) Experimental design showing cell aggregates cultured in GK15 medium supplemented with low dosage of BMP4, BMP8a, EGF and SCF. (B) FACS analysis for SSEA1 and CD61 performed at d6 on wt, Δ*Obs* and *Otx2KO* cell aggregates. (C) RT-qPCR analysis performed at d6 on SSEA1$^{+}$-CD61$^{+}$ purified cells to assess the expression level of *Blimp1*, *Ap2γ*, *Nanos3*, *Prdm14*, *Kit*, *Gcna1*, *Prmt5*, *DAZL* (also known as *DAZLA)*, *Ddx4* (also known as *Mvh*), *ALPL* (also known as *TNAP*) and *Fragilis* in wt, Δ*Obs* and *Otx2KO* cell aggregates cultured according to protocols 1 and 9. Data were normalized to *TBP* mRNA and reported as the mean ± SD of 3 independent experiments. (D) Experimental design showing cell aggregates cultured in GK15 medium supplemented with CHIR and low dosage of BMP4, BMP8a, EGF and SCF. (E) FACS analysis for SSEA1 and CD61 performed at d6 on wt, Δ*Obs* and *Otx2KO* cell aggregates.

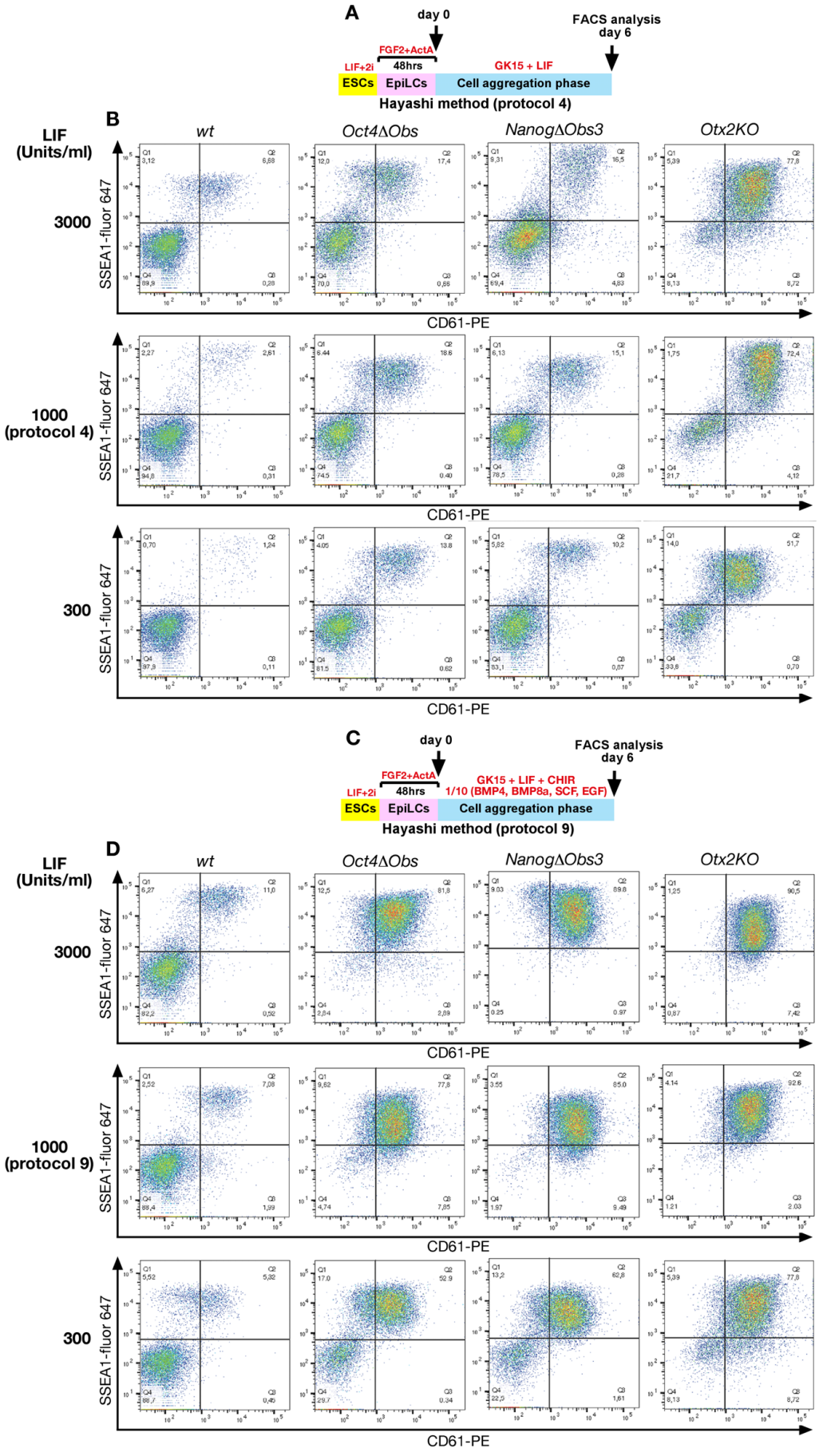


**Figure S7. Concentration-dependent effects of LIF alone and LIF in combination with CHIR and low dosage of BMP4, BMP8a, EGF and SCF.** (A) Experimental design showing cell

aggregates cultured in GK15 medium supplemented with LIF (protocol 4). (B) FACS analysis for SSEA1 and CD61 performed at d6 on wt, Δ*Obs* and *Otx2KO* cell aggregates cultured in presence of the indicated concentrantions of LIF. (C) Experimental design showing cell aggregates cultured in GK15 medium supplemented with LIF in combination with CHIR and low dosage of BMP4, BMP8a, EGF and SCF (protocol 9). (D) FACS analysis for SSEA1 and CD61 performed at d6 on wt, Δ*Obs* and *Otx2KO* cell aggregates cultured in presence of the indicated concentrantions of LIF in combination with fixed concentrations of CHIR and low dosage of BMP4, BMP8a, EGF and SCF, corresponding to those employed in protocol 9. Note that the assays with 1000 U/ml of LIF are identical to protocol 4 (B) and protocol 9 (D) culture conditions.

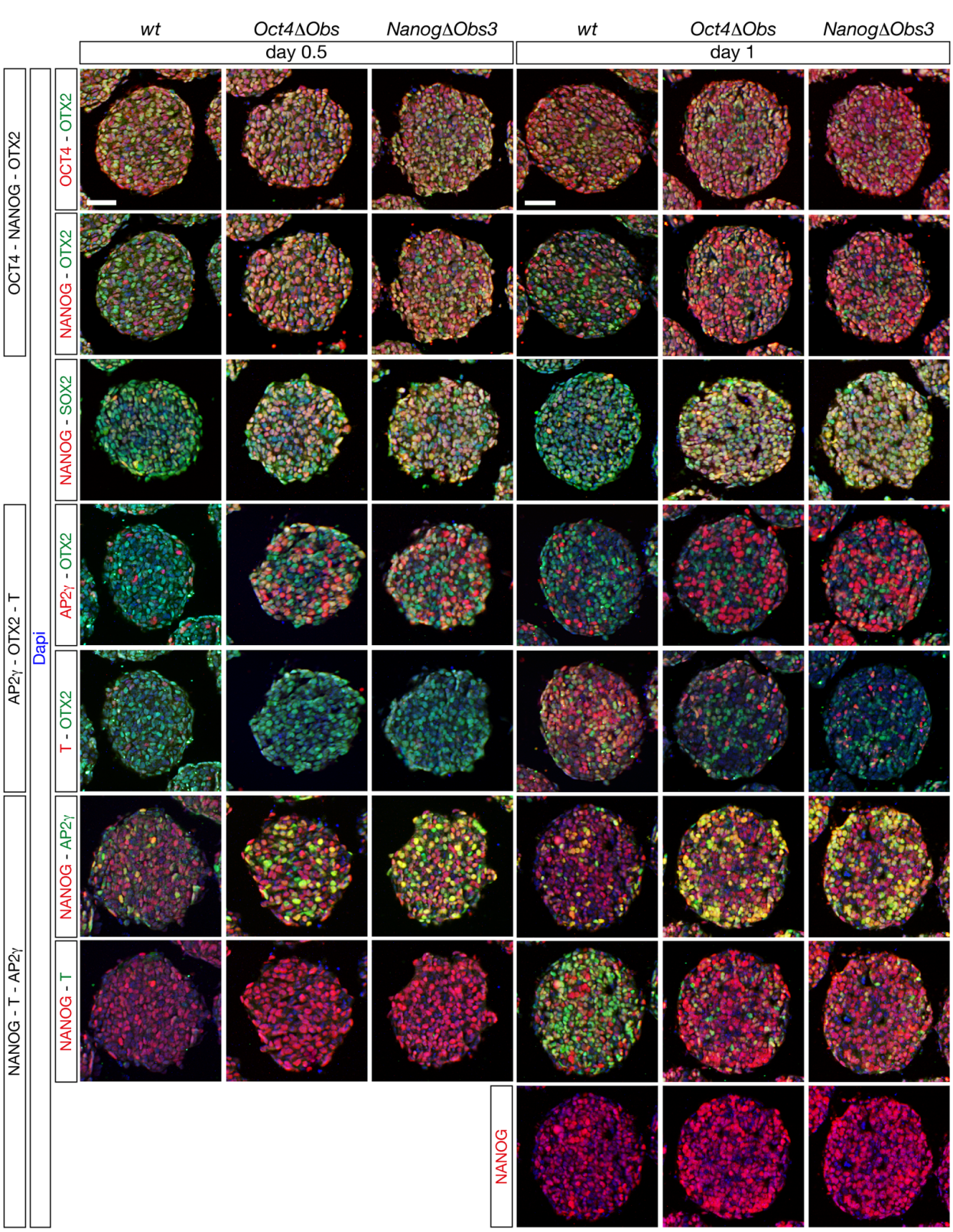


**Figure S8. Expression analysis in wt and Δ*Obs* differentiating cell aggregates.** Immunohistochemistry analysis performed at d0.5 and d1 in wt and Δ*Obs* cell aggregates generated according to the Hayashi procedure (protocol 1) with OTX2, OCT4 and NANOG, with SOX2 and NANOG, with OTX2, AP2γ and T and with NANOG, AP2γ and T. Immunostainings were performed on 3 independent experiments. Sections were counterstained with Dapi. Scale bar = 50 µm.

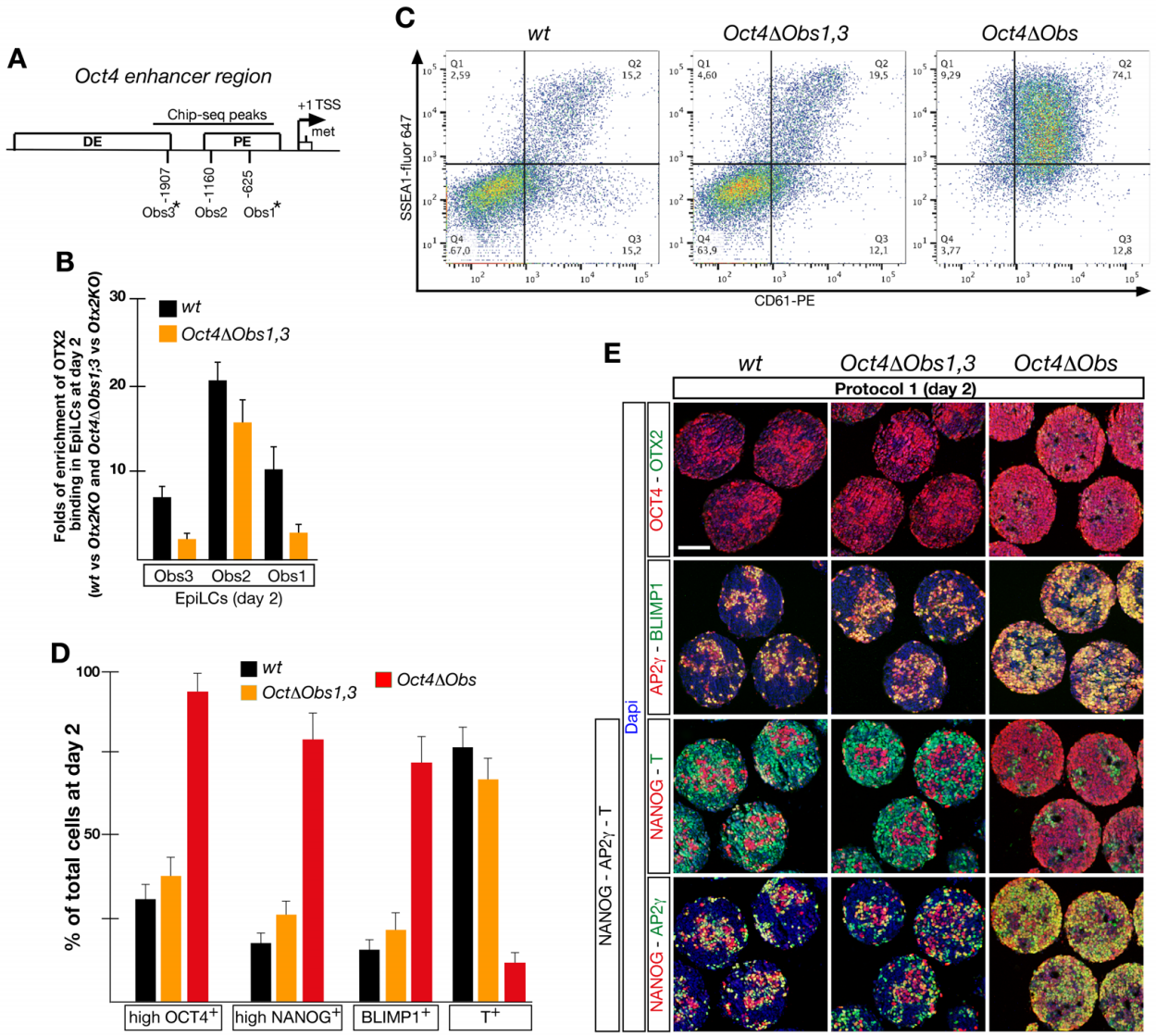


**Figure S9. Reversion to the Obs2 wt sequence in the *Oct4* enhancer region rescues wt-like generation of PGCLCs and somatic precursors.** (A) Schematic representation of the genomic region located upstream to the *Oct4* transcription start site (TSS) showing the position of PE, DE and Obs1-3; Obs1* and Obs3* correspond to the mutagenized sites of the *Oct4ΔObs1,3* mutant. (B) ChIP analysis showing that compared to wt EpiLCs, in *Oct4ΔObs1,3* mutant the OTX2 binding activity was largely recovered only for Obs2. (C) FACS analysis performed at d6 on wt, *Oct4ΔObs1,3* and *Oct4ΔObs* cell aggregates cultured according to protocol 1 showed that compared to wt, the percentage of living cells co-expressing SSEA1 and CD61 was slightly increased in *Oct4ΔObs1,3* cells. (D) Cell counting analysis performed at d2 on wt, *Oct4ΔObs1,3* and *Oct4ΔObs* cell aggregates showed that the percentage of total cells expressing high OCT4, high NANOG, BLIMP1 and T was similar in wt and *Oct4ΔObs1,3*. Data were collected from 3 independent experiments and reported as mean ± SD. Note that for wt and *Oct4ΔObs* cell counting, we included the same data as reported in Fig. 2d. (E) Representative immunohistochemistry experiments performed at d2 with the indicated antibodies on wt, *Oct4ΔObs1,3* and *Oct4ΔObs* sections from cell aggregates cultured according to protocol 1. Sections were counterstained with Dapi. Scale bar = 100µm.

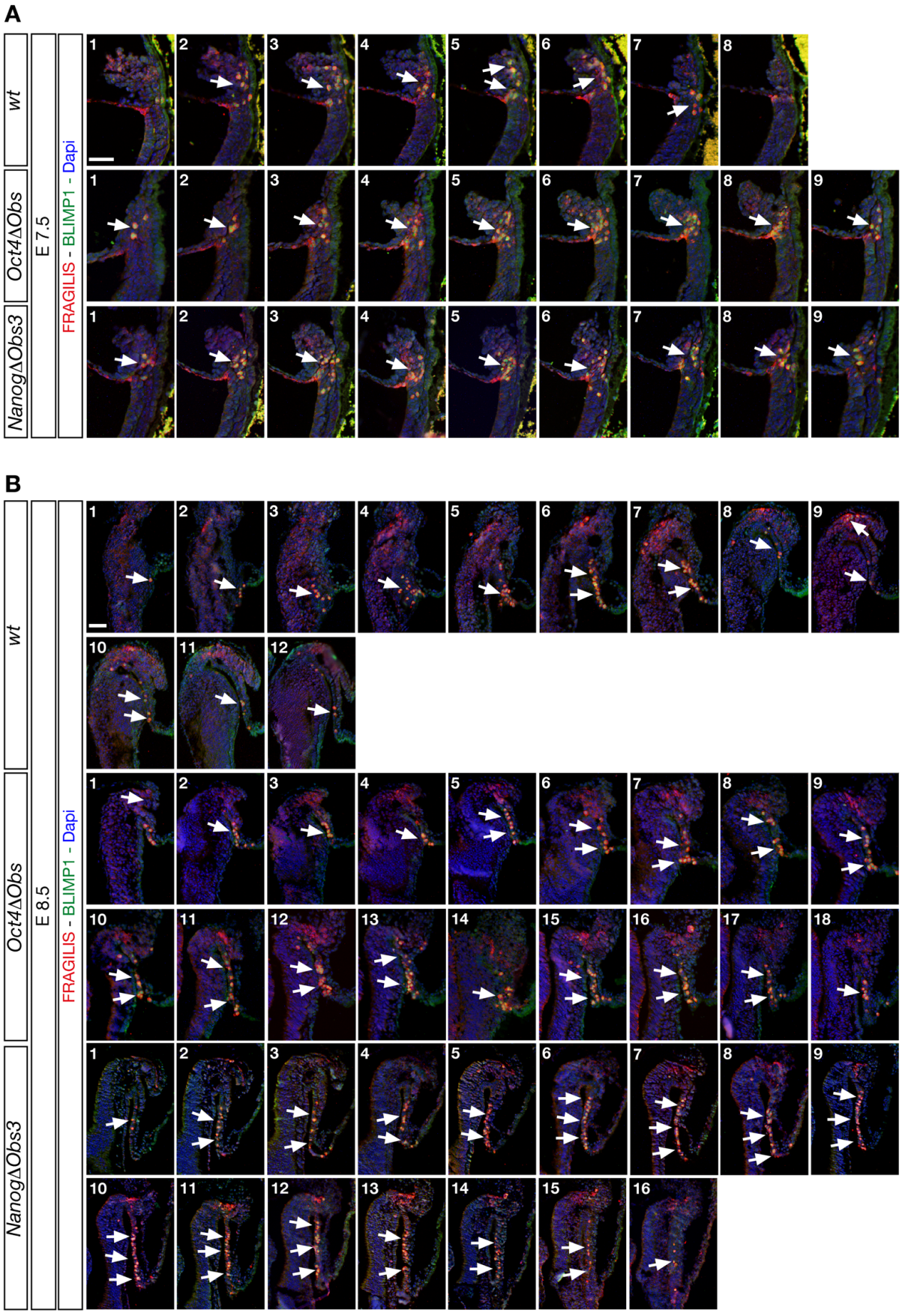


**Figure S10. PGC counting in wt and Δ*Obs* embryos.** (A-B) Sagittal sequential sections of morphologically matched E7.5 (A) and E8.5 (B) wt and Δ*Obs* embryos were immunostained with BLIMP1 and FRAGILIS to detect, virtually, all PGCs. All sections including PGCs were sequentially

numbered. Note that, mainly for E8.5 embryos, the number of mutant sections containing PGCs was reproducibly higher in mutants than in wt embryos. Arrows point to PGCs. Images in (A) corresponded to magnifications of the posteriormost region including the allantois; images in (B) included the hindgut region of the posterior embryo. Sections were counterstained with Dapi. Scale bars = 50µm.

# SUPPLEMENTARY TABLES

## Table S1. Counting of ALP$^+$ colonies in *wt* and *Oct4ΔObs* ESCs

| | Undifferentiated ESC colonies (x10$^3$ plated ESCs) (mean ± SD) | |
|---|---|---|
| Genotype | N° of Exps | Uniform ALP$^+$ |
| *wt* | 3 | 211±36 |
| *Oct4ΔObs* | 3 | 230±25 |

## Table S2. Cell counting in *wt, Oct4ΔObs, NanogΔObs3, Otx2KO* and *Oct4ΔObs1,3* cell aggregates at d2

**Number and percentage (mean ± SD) of cells expressing high NANOG, T, high OCT4 and BLIMP1; DNA is stained with Dapi**

| **Protocol 1** Genotype | N° of Exps | Total cells | high NANOG⁺ N° of cells | high NANOG⁺ % of total cells | T⁺ N° of cells | T⁺ % of total cells | Total cells | high OCT4⁺ N° of cells | high OCT4⁺ % of total cells | BLIMP1⁺ N° of cells | BLIMP1⁺ % of total cells |
|---|---|---|---|---|---|---|---|---|---|---|---|
| *wt* | 3 | 3482±98 | 747±119 | 21±3 | 2662±203 | 76±6 | 4148±179 | 1324±206 | 32±5 | 660±118 | 16±3 |
| *Oct4ΔObs* | 3 | 3786±346 | 2989±301 | 79±8 | 461±121 | 12±3 | 4248±268 | 4022±230 | 95±5 | 3050±357 | 72±8 |
| *NanogΔObs3* | 3 | 3672±49 | 3037±214 | 83±6 | 118±60 | 3±2 | 4103±244 | 3977±113 | 97±3 | 3168±357 | 77±9 |
| *Otx2KO* | 3 | 3383±271 | 3084±262 | 91±8 | 13±4 | 0,4±0,1 | 4453±121 | 4381±91 | 98±2 | 3868±321 | 87±7 |
| *Oct4ΔObs1,3* | 3 | 3579±261 | 923±157 | 26±4 | 2388±261 | 67±7 | 3541±118 | 1365±167 | 38±5 | 778±168 | 22±5 |

| **Protocol 3** Genotype | N° of Exps | Total cells | high NANOG⁺ N° of cells | high NANOG⁺ % of total cells | T⁺ N° of cells | T⁺ % of total cells | Total cells | high OCT4⁺ N° of cells | high OCT4⁺ % of total cells | BLIMP1⁺ N° of cells | BLIMP1⁺ % of total cells |
|---|---|---|---|---|---|---|---|---|---|---|---|
| *wt* | 3 | 3359±98 | 49±13 | 1±0,4 | 911±136 | 27±4 | 2742±128 | 175±36 | 6±1 | 9±2 | 0,3±0,01 |
| *Oct4ΔObs* | 3 | 2895±120 | 371±86 | 13±3 | 211±59 | 7±2 | 2663±109 | 637±102 | 24±4 | 110±28 | 4±1 |
| *NanogΔObs3* | 3 | 2837±567 | 737±139 | 26±5 | 86±26 | 3±1 | 2757±130 | 1603±228 | 58±8 | 53±19 | 2±1 |
| *Otx2KO* | 3 | 3087±204 | 1430±148 | 46±5 | 7±1 | 0,2±0,05 | 2517±68 | 1311±162 | 52±6 | 855±157 | 34±6 |

| **Protocol 4** Genotype | N° of Exps | Total cells | high NANOG⁺ N° of cells | high NANOG⁺ % of total cells | T⁺ N° of cells | T⁺ % of total cells | Total cells | high OCT4⁺ N° of cells | high OCT4⁺ % of total cells | BLIMP1⁺ N° of cells | BLIMP1⁺ % of total cells |
|---|---|---|---|---|---|---|---|---|---|---|---|
| *wt* | 3 | 3349±94 | 379±108 | 11±3 | 267±71 | 8±2 | 3513±176 | 601±107 | 17±3 | 102±33 | 3±1 |
| *Oct4ΔObs* | 3 | 3491±207 | 1547±272 | 44±8 | 11±5 | 0.3±0.1 | 3472±178 | 2161±201 | 62±6 | 657±122 | 19±4 |
| *NanogΔObs3* | 3 | 3479±185 | 1416±212 | 41±6 | 46±18 | 1±0.5 | 3475±168 | 2884±254 | 83±7 | 560±102 | 16±3 |
| *Otx2KO* | 3 | 3595±110 | 2812±261 | 78±7 | 4±2 | 0.1±0.07 | 3553±203 | 3086±204 | 87±6 | 2592±215 | 73±6 |

| **Protocol 5** Genotype | N° of Exps | Total cells | high NANOG⁺ N° of cells | high NANOG⁺ % of total cells | T⁺ N° of cells | T⁺ % of total cells | Total cells | high OCT4⁺ N° of cells | high OCT4⁺ % of total cells | BLIMP1⁺ N° of cells | BLIMP1⁺ % of total cells |
|---|---|---|---|---|---|---|---|---|---|---|---|
| *wt* | 3 | 2865±225 | 225±28 | 8±1 | 1887±223 | 66±8 | 2918±189 | 448±98 | 15±3 | 172±36 | 6±1 |
| *Oct4ΔObs* | 3 | 2910±237 | 762±169 | 26±6 | 1291±212 | 44±7 | 2794±161 | 1280±152 | 46±5 | 572±141 | 20±5 |
| *NanogΔObs3* | 3 | 2956±214 | 950±207 | 32±7 | 1573±217 | 53±7 | 2934±208 | 2147±198 | 73±7 | 792±200 | 27±7 |
| *Otx2KO* | 3 | 2649±176 | 1978±247 | 75±9 | 289±104 | 11±4 | 2758±170 | 2380±204 | 88±7 | 1719±220 | 62±8 |

## Table S3. Cell counting in *wt, Oct4ΔObs, NanogΔObs3, and Otx2KO* cell aggregates at d2

**Number and percentage (mean ± SD) of cells expressing high NANOG, T, high OCT4 and BLIMP1; DNA is stained with Dapi**

| **Protocol 6** Genotype | N° of Exps | Total cells | high NANOG⁺ N° of cells | high NANOG⁺ % of total cells | T⁺ N° of cells | T⁺ % of total cells | Total cells | high OCT4⁺ N° of cells | high OCT4⁺ % of total cells | BLIMP1⁺ N° of cells | BLIMP1⁺ % of total cells |
|---|---|---|---|---|---|---|---|---|---|---|---|
| *wt* | 3 | 3648±93 | 19±6 | 0.5±0.1 | 2230±291 | 61±8 | 3691±95 | 119±29 | 3±1 | 4±1 | 0.1±0.04 |
| *Oct4ΔObs* | 3 | 3358±74 | 535±118 | 16±4 | 381±64 | 11±2 | 3231±104 | 1110±191 | 34±6 | 158±49 | 5±2 |
| *NanogΔObs3* | 3 | 3562±128 | 400±86 | 11±2 | 560±119 | 16±3 | 3498±198 | 978±140 | 28±4 | 107±30 | 3±1 |
| *Otx2KO* | 3 | 3156±60 | 2309±246 | 73±8 | 132±53 | 4±2 | 3541±95 | 3113±240 | 88±7 | 1807±206 | 51±6 |

| **Protocol 7** Genotype | N° of Exps | Total cells | high NANOG⁺ N° of cells | high NANOG⁺ % of total cells | T⁺ N° of cells | T⁺ % of total cells | Total cells | high OCT4⁺ N° of cells | high OCT4⁺ % of total cells | BLIMP1⁺ N° of cells | BLIMP1⁺ % of total cells |
|---|---|---|---|---|---|---|---|---|---|---|---|
| *wt* | 3 | 2271±86 | 298±74 | 13±3 | 1652±176 | 73±8 | 3121±174 | 433±93 | 14±3 | 216±64 | 7±2 |
| *Oct4ΔObs* | 3 | 2260±203 | 1697±219 | 64±8 | 245±90 | 9±3 | 3107±146 | 2138±246 | 69±8 | 1626±200 | 52±6 |
| *NanogΔObs3* | 3 | 2497±163 | 1405±172 | 56±7 | 135±28 | 5±1 | 2903±145 | 2199±209 | 76±7 | 1201±176 | 41±6 |
| *Otx2KO* | 3 | 2461±264 | 2165±152 | 88±6 | 4±1 | 0,1±0,06 | 2587±160 | 2414±137 | 93±5 | 1997±180 | 77±7 |

| **Protocol 8** Genotype | N° of Exps | Total cells | high NANOG⁺ N° of cells | high NANOG⁺ % of total cells | T⁺ N° of cells | T⁺ % of total cells | Total cells | high OCT4⁺ N° of cells | high OCT4⁺ % of total cells | BLIMP1⁺ N° of cells | BLIMP1⁺ % of total cells |
|---|---|---|---|---|---|---|---|---|---|---|---|
| *wt* | 3 | 4271±86 | 585±83 | 14±2 | 2962±313 | 69±7 | 4125±127 | 943±168 | 23±4 | 330±45 | 8±1 |
| *Oct4ΔObs* | 3 | 4660±203 | 3267±413 | 70±9 | 521±161 | 11±3 | 4025±132 | 3551±311 | 88±8 | 2446±317 | 61±8 |
| *NanogΔObs3* | 3 | 4496±163 | 2915±307 | 65±7 | 805±240 | 18±5 | 4339±82 | 4075±269 | 94±6 | 2091±290 | 48±7 |
| *Otx2KO* | 3 | 4361±265 | 3668±262 | 84±6 | 54±24 | 1±0.5 | 4273±107 | 4105±156 | 96±4 | 3416±261 | 80±6 |

| **Protocol 9** Genotype | N° of Exps | Total cells | high NANOG⁺ N° of cells | high NANOG⁺ % of total cells | T⁺ N° of cells | T⁺ % of total cells | Total cells | high OCT4⁺ N° of cells | high OCT4⁺ % of total cells | BLIMP1⁺ N° of cells | BLIMP1⁺ % of total cells |
|---|---|---|---|---|---|---|---|---|---|---|---|
| *wt* | 3 | 2868±104 | 490±94 | 17±3 | 1998±197 | 70±7 | 2874±250 | 753±107 | 26±4 | 347±83 | 12±3 |
| *Oct4ΔObs* | 3 | 2772±265 | 2106±258 | 76±9 | 418±111 | 15±4 | 2723±141 | 2332±217 | 86±8 | 1880±222 | 69±8 |
| *NanogΔObs3* | 3 | 2825±182 | 2294±169 | 81±6 | 58±24 | 2±1 | 2389±179 | 2217±97 | 93±4 | 1814±146 | 76±6 |
| *Otx2KO* | 3 | 2791±150 | 2590±117 | 93±4 | 7±1 | 0.25±0.04 | 2375±241 | 2227±146 | 94±6 | 2009±172 | 84±7 |

## Table S4. PGC counting in *wt, Oct4ΔObs* and *NanogΔObs3* embryos

| Genotype | Total number of PGCs detected in wt and mutant embryos | | | |
|---|---|---|---|---|
| | N° of Embryos (E7.5) | Fragilis⁺ - Blimp1⁺ N° of PGCs (mean ± SD) | N° of Embryos (E8.5) | Fragilis⁺ - Blimp1⁺ N° of PGCs (mean ± SD) |
| *wt* | 6 | 64±10 | 7 | 148±20 |
| *Oct4ΔObs* | 6 | 95±13 | 7 | 222±38 |
| *NanogΔObs3* | 6 | 101±9 | 7 | 234±30 |

## Table S5. Primers used in this study

| Genotyping | Forward | Reverse | Size (base pairs) |
|---|---|---|---|
| *Otx2-ER* | AGGACCAAACTGCCTCTTGGAAGC | CAAAGGTTGGCAGCTCTCATGTC | 172 |
| *Ng-Obs3* (wt) | TATCTGTGAGCACAAGGACTGA | CCTGTGAATTCACAGTTAATCCC | 854 |
| *Ng-Obs3* (mutant) | TATCTGTGAGCACAAGGACTGA | CCTGTGAATTCACAGAACTGTCG | 854 |
| *Oct4-Obs1* (wt) | CCTTGCAGACAGGCACTCTGAG | CTTGTGTTGTCCAGGTTGGTAGAT | 696 |
| *Oct4-Obs1** (mutant) | CCTTGCAGACAGGCACTCTGAG | GTGTTGTCCAGGTTGGTAACAGC | 693 |
| *Oct4-Obs2* (wt) | GGTTGGTATTGAATACAGACAGGAC | GGAAAGACACTAAGGAGACGGGAT | 1025 |
| *Oct4-Obs2** (mutant) | GGTTGGTATTGAATACAGACAGGAC | GGAAAGACACTAAGGAGACTGACA | 1025 |
| *Oct4-Obs3* (wt) | TCTCGTCCTAGCCCTTCCTTAATC | TGCTGGCGGAAAGACACTAAG | 796 |
| *Oct4-Obs3** (mutant) | CGTCCTAGCCCTTCCTGCTGT | TGCTGGCGGAAAGACACTAAG | 796 |
| **RT-qPCR** | | | |
| *TBP* | GGGGAGCTGTGATGTGAAG | CCAGGAAATAATTCTGGCTCA | 93 |
| *Otx2* | TTGCCAAGACCCGGTACCCA | AACCATACCTGCACCCTGGATTCTG | 88 |
| *Oct4 (Pou5f1)* | CCTGGGCGTTCTCTTTGGAAAGGT | CAGGGGCCGCAGCTTACACA | 100 |
| *Nanog* | TGAAGTGCAAGCGGTGGCAGA | CCACTGGTGCTGAGCCCTTCTGA | 78 |
| *T (Brachyury)* | TCCCAATGGGGGTGGCTTGTT | TGGAGGGGAGAGAGAGCGAGC | 94 |
| *Ap2γ (Tfap2c)* | AGTAAAGCGGTGGCTGACT | CAGTGAACTCCTTGCACACCTGC | 116 |
| *Blimp1 (Prdm1)* | TTCTCTTGGAAAAACGTGTGGG | GGAGCCGGAGCTAGACTTG | 59 |
| *Hoxb1* | GATCCTACAGGTCTTGGGACC | AGCTCAAAGGCACTGAACTGAG | 137 |
| *Prdm14* | CATATTCTTCACGTCCATGAGAG | ATGGCCTGTCTCCAGAGTGGAC | 118 |
| *Nanos3* | GGAGCTTGATGTAAGGCTGG | TGATAGATGGCACGGGACTC | 141 |
| *ALPL (TNAP)* | TGGCTACAAGGTGGTGGAC | GGCCTGGTAGTTGTTGTGAG | 73 |
| *DAZL (DAZLA)* | TGAAGTTGATCCAGGAGCTG | GTATGCTTCGGTCCACAGAC | 107 |
| *Kit* | GAGAAGCAGATCTCGGACAG | AGTTGACCCTCACGGAATG | 106 |
| *Ddx4 (Mvh)* | TTTGCATCTGTTGACACGAG | ATCCCATGACTCGTCATCAAC | 108 |
| *Gcna1* | TTGACTCCGAATCCGACTCC | AATTAGTGGAAGCTTCTGACCTC | 122 |
| *Prmt5* | CACCAGCTCTCTGCTCCTAAG | CCATGAAGCACTGTGTTCAC | 122 |
| *Fragilis (Ifitm3)* | AACTTCTGCTGCCTGGGCTTCA | AGGCACTTAGCAGTGGAGGCGTAG | 113 |
| **ChIP-qPCR** | | | |
| *Oct4-Obs1A* | GAGCCTGGGTGCAGGTCTTAT | TGCGTTTTCAGAGCACAGTATTC | 97 |
| *Oct4-Obs2A* | AACCACTCTAGGGAAGTTCAGGG | TGCTGGCGGAAAGACACTAAG | 80 |
| *Oct4-Obs3A* | GGTTGGTATTGAATACAGACAGGAC | CCTCTAAGGCCTAGACAGCACT | 82 |
| *Oct4-DE* | GGCTGCAGGCATACTTGAAC | AGGGCAGAGCTATCATGCAC | 174 |
| *Oct4-PE* | GAAGTTCAGGGTAGGCTCTCTG | GGACTCCGGTGTTCATCCT | 113 |

## Table S6. Antibodies used in this study

### Immunohistochemistry and Immunocytochemistry

| Antigen | Source | Manufacturer | Catalog# | Dilution |
|---|---|---|---|---|
| OCT4 | Mouse | Santa Cruz Biotechnology | sc-5279 | 1:500 |
| OCT4 | Rabbit | Santa Cruz Biotechnology | sc-9081 | 1:200 |
| OCT4 | Goat | Santa Cruz Biotechnology | sc-8628 | 1:100 |
| OTX2 | Goat | R&D | AF1979 | 1:120 |
| OTX2 | Rabbit | Gift of Prof Giorgio Corte | | 1:1500 |
| NANOG | Rabbit | Cell Signaling | #8822 | 1:500 |
| OCT6 | Mouse | Millipore | MABN738 | 1:100 |
| T (BRACHYURY) | Goat | Santa Cruz Biotechnology | sc-17745 | 1:100 |
| T (BRACHYURY) | Rabbit | Abcam | Ab-209665 | 1:1000 |
| ESTROGEN RECEPTOR (ERα) | Mouse | Santa Cruz Biotechnology | sc-8002 | 1:200 |
| AP2γ | Mouse | Santa Cruz Biotechnology | sc-53162 | 1:100 |
| FRAGILIS | Goat | R&D | AF3377 | 1:100 |
| SOX2 | Goat | R&D | AF2018 | 1:100 |
| BLIMP1 | Rat | Santa Cruz Biotechnology | sc-47732 | 1:80 |

### ChIP assays

| Antigen | Source | Manufacturer | Catalog# | Dilution |
|---|---|---|---|---|
| HISTONE H3K9me3 | Rabbit | Abcam | ab-8898 | 4μg of antibody/25μg of chromatin |
| OTX2 | Rabbit | Gift of Prof Giorgio Corte | | 2.5 μl of immune serum/$10^7$ cells |

### Western Blotting

| Antigen | Source | Manufacturer | Catalog# | Dilution |
|---|---|---|---|---|
| STAT3 | Rabbit | Cell Signaling | #9132 | 1:1000 |
| p-STAT3 | Rabbit | Cell Signaling | #9131 | 1:700 |
| βCATENIN | Rabbit | Cell Signaling | #9562 | 1:1000 |
| Active βCATENIN | Mouse | Millipore | 05-665 | 1:800 |
| p-βCATENIN | Rabbit | Cell Signaling | #9561 | 1:600 |
| SMAD1 | Rabbit | Cell Signaling | #9743 | 1:1000 |
| p-SMAD1,5,8 | Rabbit | Cell Signaling | #9511 | 1:600 |
| SMAD2 | Mouse | Cell Signaling | #3103 | 1:1000 |
| p-SMAD2 | Rabbit | Cell Signaling | #3108 | 1:700 |
| ERK1,2 | Rabbit | Cell Signaling | #9102 | 1:1000 |
| p-ERK1,2 | Rabbit | Cell Signaling | #9101 | 1:700 |
| βACTIN | Mouse | Santa Cruz Biotechnology | sc-69879 | 1:5000 |

### FACS

| Antigen | Source | Manufacturer | Catalog# | Dilution |
|---|---|---|---|---|
| CD15 | Mouse | Biolegend | 125608 | 1:200 |
| CD61 | Hamster | Biolegend | 104307 | 1:500 |